

AD-771 437

INVESTIGATION OF UV PHOTOIONIZATION
SUSTAINED DISCHARGE FOR GAS LASERS

Richard Lind, et al

Hughes Research Laboratories

Prepared for:

Office of Naval Research

December 1973

DISTRIBUTED BY:

NTIS

National Technical Information Service
U. S. DEPARTMENT OF COMMERCE
5285 Port Royal Road, Springfield Va. 22151

UNCLASSIFIED

Security Classification

DOCUMENT CONTROL DATA - R&D		
(Security classification of title, body of abstract and indexing annotation must be entered when the overall report is classified)		
1. ORIGINATING ACTIVITY (Corporate author) Hughes Research Laboratories 3011 Malibu Canyon Road Malibu, CA 90265		2a. REPORT SECURITY CLASSIFICATION UNCLASSIFIED
		2b. GROUP
3. REPORT TITLE INVESTIGATION OF UV PHOTOIONIZATION SUSTAINED DISCHARGE FOR GAS LASERS		
4. DESCRIPTIVE NOTES (Type of report and inclusive dates) Semiannual Technical Report - 2 January 1973 thru 30 June 1973		
5. AUTHOR(S) (First name, middle initial, last name) Richard Lind		
6. REPORT DATE December 1973	7a. TOTAL NO. OF PAGES 65	7b. NO. OF REFS 0
8a. CONTRACT OR GRANT NO. N00014-73-C-0287	9a. ORIGINATOR'S REPORT NUMBER(S)	
b. PROJECT, TASK, WORK UNIT NOS. ARPA Order No. 1807		
c. DOD ELEMENT	9b. OTHER REPORT NO(S) (Any other numbers that may be assigned this report)	
d. DOD SUBELEMENT		
10. DISTRIBUTION STATEMENT	DISTRIBUTION STATEMENT A Approved for public release; Distribution unlimited	
11. SUPPLEMENTARY NOTES	12. SPONSORING MILITARY ACTIVITY Advanced Research Projects Agency Arlington, Virginia 22209	
13. ABSTRACT <p>The objective of this program is to investigate and improve ultraviolet (UV) photoionization plasma conditioning techniques. The primary goals of the program are the demonstration of a UV sustained electrical discharge atmospheric pressure CO₂ laser together with an understanding of the scalability limits of such a scheme. The dynamics of the plasma generation in the UV sustained scheme are similar to those of the electron beam controlled discharge. The feature which makes the UV sustained scheme an attractive system to study is its simplicity of construction as opposed to that of the e-beam.</p> <p>A test apparatus has been constructed which employs spark UV sources located adjacent to a laser cavity region. A low ionization potential organic molecule is then added to this region. With this scheme input energies in excess of 200 J/l-atm with pulse lengths longer than 50 μsec have been demonstrated. Various spectral emission and photoionization yield measurements have indicated that single step photoionization is the mechanism responsible for the production of the observed dense plasma.</p>		

AD 771437



INVESTIGATION OF UV PHOTOIONIZATION
SUSTAINED DISCHARGE FOR GAS LASERS

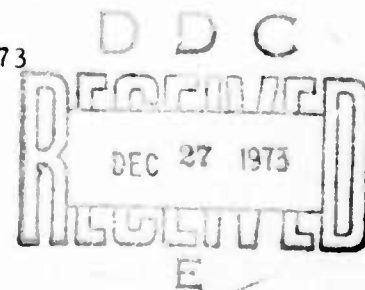
Semiannual Technical Report
Contract N00014-73-C-0287
Reporting Period: 2 January 1973 through 30 June 1973

ARPA Order No. 1807
Program Code No. 3E90

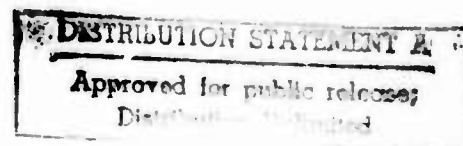
Effective Date of Contract: 2 January 1973
Contract Expiration Date: 31 December 1973

Amount of Contract: \$196,678.00
Principal Investigator: J. Y. Wada
(213) 456-6411
Principal Scientist: R. C. Lind
(213) 456-6411

Scientific Officer: Director, Physics Programs
Physical Sciences Division
Office of Naval Research
Department of the Navy
800 North Quincy Street
Arlington, Virginia 22217



Reproduced by
NATIONAL TECHNICAL
INFORMATION SERVICE
U S Department of Commerce
Springfield VA 22151



This research was supported by the Advanced Research Projects
Agency of the Department of Defense and was monitored by ONR under
Contract No. N00014-73-C-0287.

TABLE OF CONTENTS

	LIST OF ILLUSTRATIONS	v
	ABSTRACT	vi
I	INTRODUCTION	1
II	UV PHOTOIONIZATION PROCESSES AND REQUIREMENTS	3
	A. Introduction	3
	B. Single Step Ionization Model.	6
	C. Two-Step Ionization Process	11
	D. Photoabsorption in a CO ₂ Laser Medium	15
	E. Sample Calculation - NO Seeded Gas	19
III	EXPERIMENTAL PROGRAM RESULTS	29
	A. Plasma Discharge Measurements	29
	1. Sustainer Energy Results	29
	2. V-I Characteristics	42
	3. Discharge Volume Determination	42
	4. Electron Number Density Determination	44
	5. Photodissociation and Contamination Results	46
	B. Photoionization Yield Measurements	48
	C. UV Emission Spectra.	54
	D. Preliminary Small Signal Gain Measurements.	57
IV	CONCLUSIONS AND FUTURE PLANS	61

LIST OF ILLUSTRATIONS

<u>Figure</u>		<u>Page</u>
1	Simplified schematic diagram of the UV photoionization concept	4
2	Alternative Configuration for UV photoionization approach	5
3	Configuration used for photoionization analysis	7
4	A plot of the function $Si(\nu)$ as a function of l_p	10
5	Two-step photoionization processes in a seeded gas	12
6	Photo absorption cross section of CO_2	16
7	Absorption spectrum of carbon dioxide	18
8	Energy diagram of NO	20
9	The absorption spectrum of nitric oxide, NO	21
10	Absorption spectrum of NO	22
11	Simplified emission model used for analysis	26
12	Summary of photoionization in NO seeded CO_2 mixture	27
13	Photograph of test device	30
14	Schematic of UV spark and sustainer circuits	31
15	Calibration curve for hypodermic syringe, and calibration.	33
16	Oscilloscope trace of sustainer and UV current	34
17	Sustainer energy as a function of UV current for various concentrations of Tri-n-propylamine	35
18	Sustainer energy normalized to total pressure as a function of UV current for various total pressures	37
19	Sustainer energy as a function of UV current for various laser mixtures	38

<u>Figure</u>		<u>Page</u>
20	Sustainer Energy as a function of UV current for various ballast resistances	41
21	V-I characteristics of the plasma discharge	43
22	Electron number density as a function of E/N	45
23	Sustainer energy as a function of number of discharge firings	47
24	Photoionization yield test chamber	49
25	UV window transmission characteristics	50
26	Relative photoionization contribution from various wavelength regions for Tri-n-propylamine	51
27	UV photon mean free path through CO ₂ at .02 atm.	52
28	UV mean free path through Tri-n-propylamine at .3 Torr	53
29	Test setup for spark spectrum emission and absorption measurements	55
30	Relative emission spectra of a He spark discharge for three current levels	56
31	Relative emission spectra of N ₂ and He at 300 amps	56
32	Relative emission spectra of two CO ₂ /N ₂ /He laser mixtures at 300 amps	58
33	Sustainer energy measurements obtained using different emission gases	58
34	Gain measurements in UV sustained CO ₂ laser	59

ABSTRACT

The objective of this program is to investigate and improve ultraviolet (UV) photoionization plasma conditioning techniques. The primary goals of the program are the demonstration of a UV sustained electrical discharge atmospheric pressure CO₂ laser together with an understanding of the scalability limits of such a scheme. The dynamics of the plasma generation in the UV sustained scheme are similar to those of the electron beam controlled discharge. The feature which makes the UV sustained scheme an attractive system to study is its simplicity of construction as opposed to that of the e-beam.

A test apparatus has been constructed which employs spark UV sources located adjacent to a laser cavity region. A low ionization potential organic molecule is then added to this region. With this scheme input energies in excess of 200 J/l-atm with pulse lengths longer than 50 μ sec have been demonstrated. Various spectral emission and photoionization yield measurements have indicated that single step photoionization is the mechanism responsible for the production of the observed dense plasma.

I. INTRODUCTION

The objective of this program is to investigate and improve ultraviolet (UV) photoionization plasma conditioning techniques. Within the scope of this objective is the specific goal of the demonstration of a UV sustained electrical discharge atmospheric pressure CO₂ laser. The dynamics of the plasma generation in this mode are similar to those of the electron beam controlled discharge; the voltage applied to the main discharge electrodes can be reduced below that required for a self-sustained avalanche mode. The principal advantage realized in this approach is complete control of the main discharge by the UV source at all times during operation.

The attractive feature of UV sustained as opposed to e-beam sustained operation is the simplicity of construction. Specifically, a foil is not required and the high voltages needed to give efficient electron penetration of the foil are not necessary.

The crucial questions that need to be answered through the research conducted during this program are first; whether or not an electron density sufficient to sustain the discharge in a CO₂ laser mixture can be produced by a UV photoionization technique - specifically, plasma densities of 10^{12} electrons/cm³ over plus lengths of 20 μ sec or longer must be attained; and second, what are the scalability parameters for such a technique.

The program being pursued to investigate these questions consists basically of the following three tasks:

1. Determination of the emission spectrum and power saturation characteristics of UV spark sources operated in CO₂ laser mixture, metal vapors, and other gas additives.
2. Development of seeding techniques which will improve the photoionization efficiency of the laser medium.
3. Evaluation of UV photoionization sustained CO₂ laser gas discharge characteristics and laser performance via small signal gain and laser power output measurements.

The results to be discussed in this report emanate from the direction indicated by tasks one and two. The principal results to date are: emission spectra of spark discharges have been obtained; plasma densities approaching those required ($n_e = 10^{12}$ electron/cm³ for >20 μ sec) have been measured; and a tentative projection of scalability limits have been obtained. Based on these results, baseline operating conditions for laser gas mixtures, seed gas concentrations, and UV intensities have been established and will be used as a guideline for laser measurements (Task 3) and more extensive scalability studies during a portion of the remainder of the program.

II. UV PHOTOIONIZATION PROCESSES AND REQUIREMENTS

A. Introduction

In this section, we briefly review the basic processes involved and requirements associated with the production of UV photoionization sustained discharges in high pressure CO_2 lasers. A schematic configuration for the UV photoionization concept is shown in Fig. 1. A UV source is placed at some position close to the main discharge volume. The UV radiation can be provided either by an auxiliary discharge placed within the same laser gas as shown in the figure or by UV flashlamps. The UV radiation from these sources propagates into the main discharge volume and photoionizes a fixed number of neutral CO_2 laser gases and low ionization potential seed gas molecules in this region. The resulting ionization background of electrons serves to condition, both spatially and temporally, the main discharge plasma.

Several alternate configurations are possible. The spatial homogeneity of the main discharge is significantly improved by symmetrical placement of a second preionizer electrode configuration on the unilluminated sides of the main discharge as shown in Fig. 2(a). Other variations consist of using grid electrodes in the main discharge and placing the UV sources above and/or below the main discharge as shown in Fig. 2(b) and 2(c). These latter two configurations are particularly adaptable to high average power systems requiring high speed gas flow.

Once a uniform preionization background has been established, plasma conditioning in the main discharge is maintained by the application of a voltage below that required to produce avalanche condition. The dynamics of the plasma in this mode are then similar to that of the electron beam controlled sustainer discharge. In this configuration, the high energy electron beam is replaced by a low energy photon preionization source. The principal advantage realized in this mode of non-avalanche operation is the complete control of the main discharge by the preionization discharge at all times during the discharge sequence.

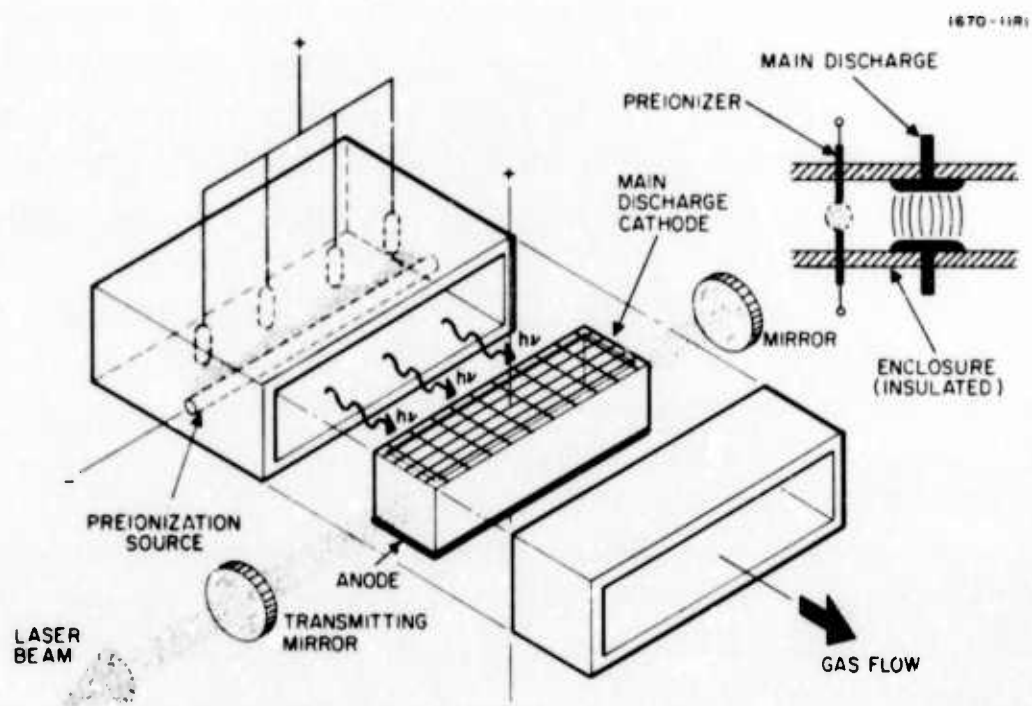
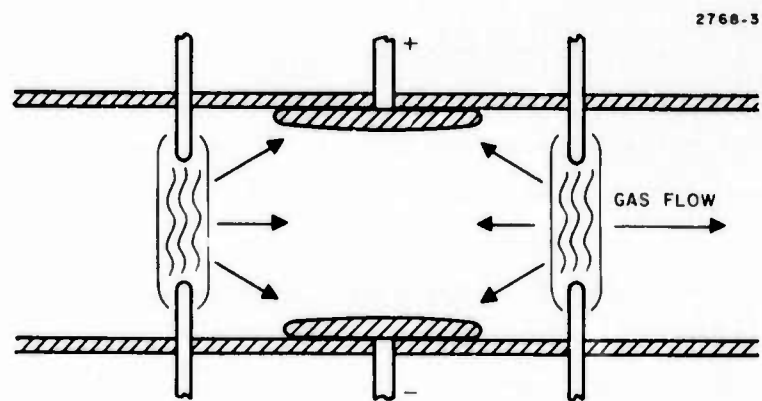
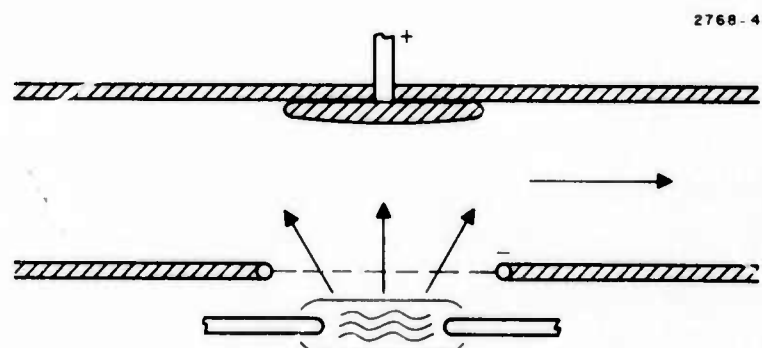


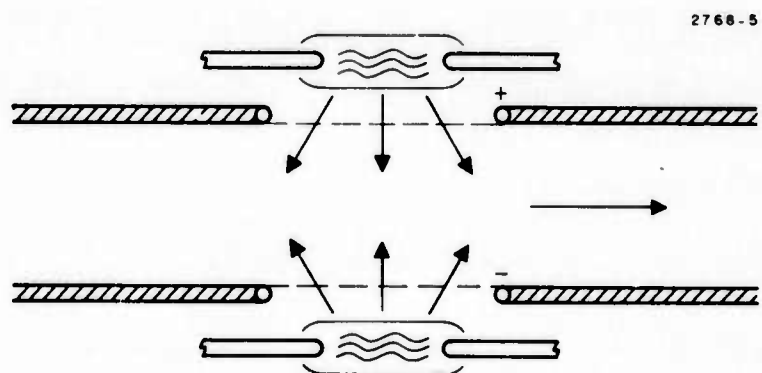
Fig. 1. Simplified schematic diagram of the UV photoionization concept.



(a)



(b)



(c)

Fig. 2. Alternative configuration for UV photoionization approach.

B. Single Step Ionization Model

The most elementary photon preionization laser configuration considered for analysis is shown in Fig. 3. We assume a point source of photons radiating a total spectral power $P(\nu, t)$. The actual source configuration may be synthesized by a superposition of such point source solutions. Later the solutions also will be generalized to cylindrical and planar sources.

The photon flux Φ with frequency ν that reaches position z is given by

$$\Phi(\nu, z, t) = \frac{P(\nu, t)}{4\pi h\nu} \frac{e^{-\mu(z)z}}{z^2} \quad (1)$$

where $\mu(z)$ is the photon attenuation per unit of length in the gas. The number of electrons $S_i(\nu, z, t)$ produced per second by direct single step photoionization in an elemental volume located at z is then

$$S_i(\nu, z, t) = \sigma_i(\nu) n_o \Phi(\nu, z, t) \quad (2)$$

where $\sigma_i(\nu)$ is the cross section for photoionization, and n_o is the gas density. It will also be useful to introduce the concept of a photon mean free path $\ell_p(\nu)$ through the relation

$$\frac{1}{\ell_p(\nu)} \equiv \sigma_i(\nu) n_o = \mu(\nu) \quad (3)$$

The total electron generation rate is given by the sum of all spectral contributions from the source

$$S_i(z, t) = \int_0^\infty S_i(\nu, z, t) d\nu \quad (4)$$

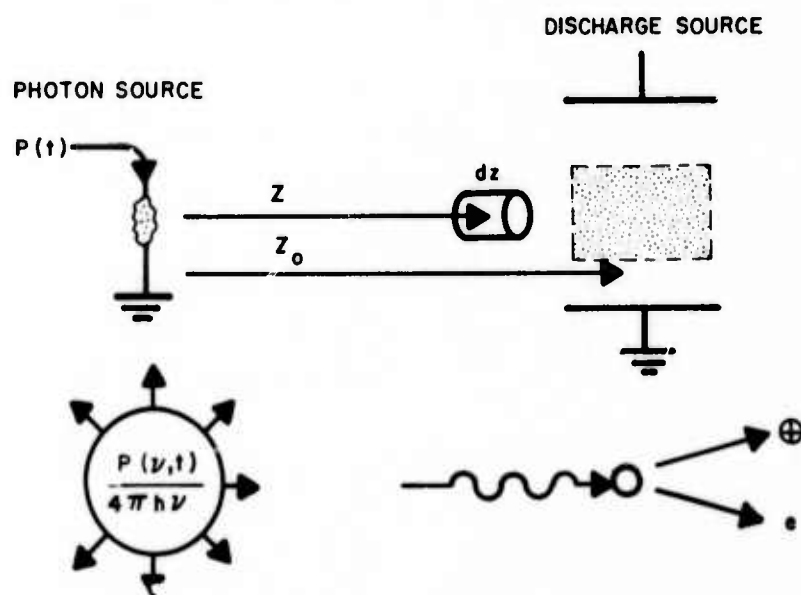


Fig. 3. Configuration used for photoionization analysis.

The quantity of prime interest is the photoelectron density $n_e(z, t)$ generated by the preionizer source. This quantity is obtained by solving

$$\frac{\partial n_e}{\partial t}(z, t) = S_i(z, t) - \alpha n_e^2 - \beta n_e + D \nabla^2 n_e \quad (5)$$

The dominant loss mechanisms for electrons are due to recombination (αn_e^2) and attachment (βn_e). Diffusion effects ($D \nabla^2 n_e$) can be neglected at high gas pressures. Partial solutions for this differential equation are given in Table I.

The value of the photoelectron density at any position z is related to the photoelectron generation rate $S_i(\nu, z, t)$. Substituting eqs. (2) and (3) into eq. (1) yields the relation

$$S_i(\nu, z, t) \propto \frac{\exp[-\ell/\ell_p]}{z^2} \quad (6)$$

One notes that $S_i(\nu, z, t)$ is only a function of the photon mean free path ℓ_p , if we assume that the cross sections for photoionization σ_i and photoabsorption σ_a are equal. This functional relationship is shown in Fig. 4. Maximum ionization occurs when ℓ_p is equal to the distance to the observation point. If $\ell_p/z > 1$, the absorption of the photon flux is reduced but so is the photoionization cross section; thus, $S_i(\nu)$ decreases. The opposite situation occurs if $\ell_p/z < 1$. It should also be noted that $S_i(\ell_p)$ decreases at a much greater rate if $\ell_p/z < 1$ than in the opposite limit where $\ell_p/z > 1$. This behavior will significantly influence the choice of ℓ_p/z required for optimum homogeneity of the photoelectron spatial distribution.

Substituting the optimum value of ℓ_p into eq. (6), the maximum value of the photoelectron generation rate $S_i(\text{max.})$ for a given photon frequency ν may be written in the form

$$S_i(\text{max.}) = \frac{P(\nu)}{4\pi h\nu} \frac{0.37}{z_o^n} \quad (7)$$

where $n = 3, 2$, or 1 for a point, line, or planar source, respectively. The necessity for uniform photon illumination is apparent for attainment of maximum electron density. The above result will change somewhat depending on the exact relationship of σ_i to σ_a , (see Section III). The general behavior will be preserved, however.

TABLE I
Photoelectron Density Relationship in
Recombination and Attachment Dominated Cases

	Recombination Dominated Case	Attachment Dominated Case
Electron density [$n_e(z, t)$]	$n_e(\text{max}) \tanh \frac{t}{t_r}$	$n_e(\text{max}) \left(1 - e^{-\frac{t}{t_r}} \right)$
Max. electron density [$n_e(\text{max})$]	$\left(\frac{Si}{\alpha} \right)^{1/2}$	$\left(\frac{Si}{\beta} \right)$
Rise time (t_r)	$\frac{1}{(\alpha Si)^{1/2}}$	$\left(\frac{1}{\beta} \right)$
Decay time (t_D)	$\frac{1}{\alpha n_e(z, t)} = t_\alpha$	$\left(\frac{1}{\beta} \right) = t_\beta$
$\alpha \equiv$ Recombination coefficient $\beta \equiv$ Attachment coefficient $Si \equiv$ Photoionization Rate		

T740

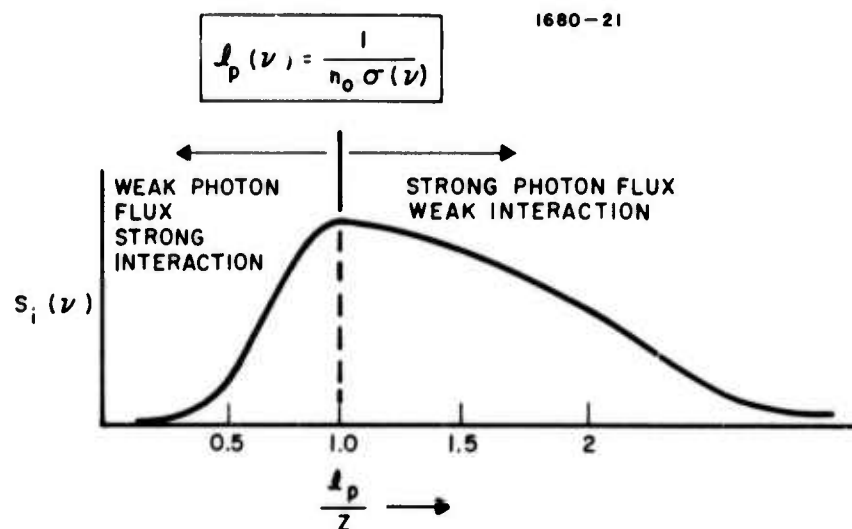


Fig. 4. A plot of the function $S_i(\nu)$ as a function of ℓ_p .

C. Two-Step Ionization Process

In the multi-step process, the first step is a photoinduced transition to an intermediate excited state in the molecule and the second or third step being a photoinduced transition from the excited state to the ionization continuum. Consider a two-state system where N_0 and N_1 are the population density in the ground and excited states respectively. Let ϕ_0 and ϕ_1 be the photon flux densities at frequencies ν_0 and ν_1 that pump the excited level and the ionization continuum as shown in Fig. 5. If the cross-sections for photoexcitation and ionization are σ_0 and σ_1 , respectively, the equation governing N_1 and the photoelectron density n_e are

$$\frac{dN_1}{dt} = N_0\sigma_0\phi_0 - \frac{N_1}{\tau_1} - N_1\sigma_1\phi_1 \quad (8)$$

$$\frac{dn_e}{dt} = N_1\sigma_1\phi_1 - \alpha n_e^2 - \beta n_e \quad (9)$$

where τ is the lifetime of the intermediate excited states, α is the electron-ion recombination coefficient and β is the attachment coefficient. Here again like in the single step process, the terms N_1 , n_e , ϕ_0 and ϕ_1 are functions of the spatial coordinates. The term $N_1\sigma_1\phi_1$ in eq. (8) takes into account the loss of molecules in the excited state due to photoionization.

If we assume ϕ_0 and ϕ_1 are applied at $t = 0$ and are slowly varying functions in time, the solution of eq. (8) becomes

$$N_1 = \frac{N_0\sigma_0\phi_0\tau_1}{(1 + \sigma_1\phi_1\tau_1)} \left[1 - e^{-(1 + \sigma_1\phi_1\tau_1)t/\tau_1} \right]. \quad (10)$$

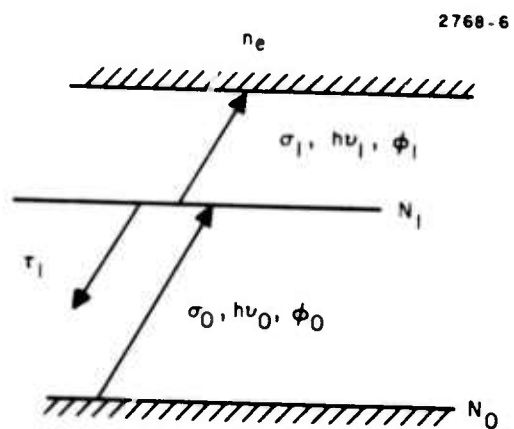


Fig. 5. Two-step photoionization processes in a seeded gas.

For $t \gg \tau_1$, the maximum steady state density of the excited level is given by

$$N_{1(\max)} = \frac{N_0 \sigma_0 \phi_0 \tau_1}{(1 + \sigma_1 \phi_1 \tau_1)} . \quad (11)$$

Note that as $\phi_1 \sigma_1$ becomes greater than $1/\tau_1$, the value of $N_{1(\max)}$ decreases. This condition requires a relatively large UV photon flux density (ϕ_1). For a case with $\sigma_1 \approx 10^{-17} \text{ cm}^2$ and $\tau_1 \approx 10^{-6} \text{ sec}$, the crossover point occurs when $\phi_1 \approx 1/\sigma_1 \tau_1 \approx 10^{-24} \text{ photons/cm}^2$, or 1 MW/cm^2 of photons in the 2000 \AA wavelength range. If the relaxation time τ_1 is larger, the crossover point would occur at a correspondingly smaller ϕ_1 value.

1. Partial Solutions for $(1/\tau_1) \ll \sigma_1 \phi_1$

In the limit where $(1/\tau_1) \ll \sigma_1 \phi_1$, the intermediate excited state simply becomes

$$N_{1(\max)} = N_0 \cdot \frac{\sigma_0 \phi_0}{\sigma_1 \phi_1} . \quad (12)$$

Substituting this equation into eq. (9), we obtain two solutions:

Recombination Dominated Case:

$$n_e(t) = n_e(\max)_\alpha \tanh \left(\frac{t}{t_\alpha} \right) \quad (13)$$

where

$$\left. \begin{aligned} n_e(\max)_\alpha &= \left(\frac{\tau_1 N_0 \sigma_0 \sigma_1 \phi_0 \phi_1}{\alpha} \right)^{1/2} \\ t_\alpha &= \frac{1}{\alpha n_e(\max)_\alpha} \end{aligned} \right\} \quad (14)$$

Attachment Dominated Case:

$$n_e(t) = n_e(\max)_\beta \left[1 - \exp \left(\frac{-t}{t_\beta} \right) \right] \quad (15)$$

where

$$\left. \begin{aligned} n_e(\max)_\beta &= \frac{\tau_1 N_0 \sigma_0 \sigma_1 \phi_0 \phi_1}{\beta} \\ t_\beta &= \frac{1}{\beta} \end{aligned} \right\} \quad (16)$$

These expressions reduce to the same form as those solutions of single step ionization process discussed before.

2. Partial Solutions for $(1/\tau_1) \gg \sigma_1 \phi_1$

In the opposite limit $(1/\tau_1 \gg \sigma_1 \phi_1)$, the solution takes on a simpler form:

Recombination Dominated Case:

$$\left. \begin{aligned} n_e(t) &= n_e(\max)_\alpha \tanh \left(\frac{t}{t_\alpha} \right) \\ n_e(\max)_\alpha &= \left(\frac{N_0 \sigma_0 \phi_0}{\alpha} \right)^{1/2} \\ t_\alpha &= \frac{1}{\alpha n_e(\max)_\alpha} \end{aligned} \right\} \quad (17)$$

where

and

Attachment Dominated Case:

$$n_e(t) = n_e(\max)_\beta \left[1 - \exp\left(\frac{-t}{t_\beta}\right) \right]$$

$$n_e(\max)_\beta = \frac{N_0 \sigma_0 \phi_0}{\beta} \quad (18)$$

$$t_\beta = \frac{1}{\beta}$$

In the last two equations, the terms related to photoionization of the excited state do not appear. This results from the fact that the excited state is efficiently pumped to ionization continuum by an intense UV radiation. The net photoionization rate is simply controlled in this case by the generation rate of the intermediate state.

Up to this point, we have assumed that the photon radiation coincided with a one-to-one correspondence in frequency with the molecular transition. Furthermore, we have assumed that the involved two-step process resulted from a single excited state. Neither of these conditions is completely satisfied in the high pressure CO_2 laser environment. As will be discussed later, the emission spectrum of UV sources consists generally of broad background with pressure broadened discrete peaks. The photoabsorption transitions in a seeded CO_2 mixture generally consist of many overlapping states forming a broad absorption continuum. The solutions to specific problems will require a more complete modeling of both the UV radiation spectrum and the laser medium. In our sample calculations, we have incorporated these corrections which will be mentioned as we proceed.

D. Photoabsorption in a CO_2 Laser Medium

A summary plot of the photoabsorption cross sections of the principal gas constituent (CO_2), is shown in Fig. 6 over the spectral

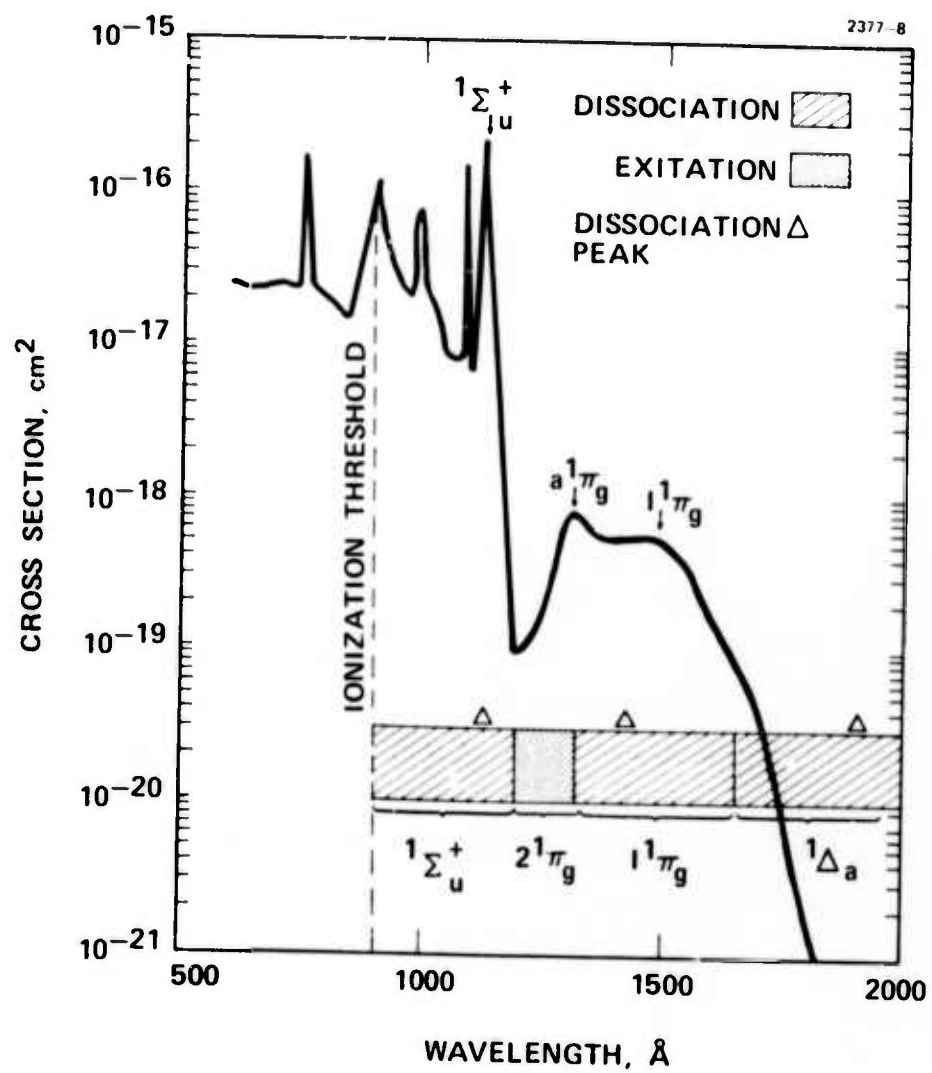


Fig. 6. Photo absorption cross section of CO_2 .

range extending from 200 to 2000 Å. For wavelengths shorter than 900 Å, the absorption in CO₂ results mainly from the photoionization process. In this region the photon mean free path (ℓ_p) is extremely short. At 1 atm, $\ell_p < 10^{-2}$ cm. Even if the gas number density of CO₂ is reduced by an order of magnitude to 0.1 atm (which is the approximate CO₂ concentration in a typical laser gas mixture), the mfp does not extend beyond a few millimeters.

In the wavelength range $\lambda > 900$ Å, the CO₂ absorption becomes a dominant factor. The absorption due to He is totally negligible, while the N₂ exhibits relatively low absorption spectra up to the 1000 to 1100 Å range, becoming totally negligible beyond this range. Summarized in Fig. 7 are the expanded absorption spectrum of CO₂ taken with a high resolution (quoted resolution of <0.2 Å) instrument. This CO₂ spectrum is characterized by a broad continuum with the transmission windows occurring at $\lambda \approx 1200$ Å and $\lambda > 1600$ Å. The short wavelength windows at 1200 Å is relatively narrow, the 1/10 power points occurring at 1160 Å and 1275 Å. The corresponding peak mfp of this window is 1 cm at 1 atm gas pressure. This mfp scales to 20 to 30 cm for the approximate CO₂ concentration of a few percent in a typical CO₂ mixture. The window at $\lambda > 1600$ Å is much broader. The corresponding mfp is about 10 cm in a CO₂ laser mixture at 1600 Å and monotonically increasing at longer wavelengths.

In the spectral region outside these two windows, the photons cannot propagate any more than a small fraction of a cm distance from the source. The photons in these opaque regions of 1100 Å and 1300 to 1600 Å cannot be used in a sizeable CO₂ laser system with cross-sectional dimensions exceeding tens of centimeters. Furthermore, the absorption spectra in these regions result from the photodissociative transitions (as identified in Fig. 6). From the practical viewpoint, it is desirable to avoid wavelengths that give rise to photodissociative reactions for many regions: (a) dissociation of the CO₂ is undesirable since the dissociation product of atomic oxygen recombine to form molecular oxygen and produces a large increase in the electron attachment coefficient in the electrical discharge; (b) since these dissociation

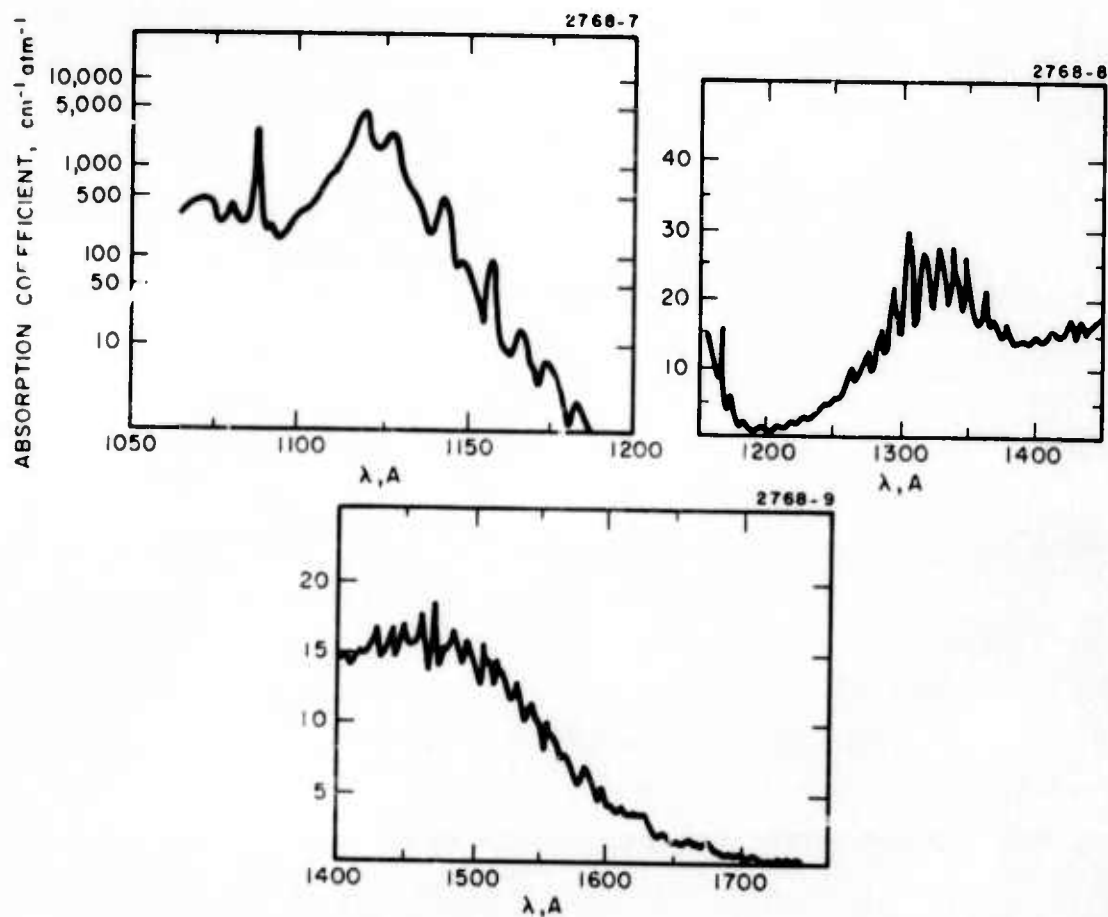


Fig. 7. Absorption spectrum of carbon dioxide.
From Inn, Watanabe, and Zelicoff.
J. Chem. Phys., 21, 1648 (1953).

states do not contribute to the photoionization processes, the photon source output should be concentrated in other useful portions of the spectrum to increase the electrical to photon conversion efficiency of the source. In the discussion to follow, we shall focus upon the two ($\lambda \approx 1200 \text{ \AA}$ and $\lambda \approx 1600 \text{ \AA}$) windows where the mfp's of the photons larger than 10 cm are feasible.

E. Sample Calculation - NO Seeded Gas

A number of low ionization organic seed gases has been used successfully for the generation of a dense plasma ($\approx 10^{12}$ electrons/cm³) in a CO₂ laser mixture. A quantitative analysis of the photoionization processes involved in many of these seeded systems has been made difficult due to the lack of pertinent data. The required lifetime information of excited states in organic molecules is simply not available. In order to circumvent this, we have sought and found nitric oxide (NO), a low ionization gas whose physical properties are well known.

The nitric oxide molecule has been investigated extensively for the past several years, owing to its importance in the upper atmosphere study. The detailed molecular energy diagram and the measured absorption spectrum of the NO molecules are shown in Figs. 8 and 9. The ionization threshold value for this molecule is 9.25 eV (or $\approx 1340 \text{ \AA}$) whereas the lowest excited state occurs in γ band ($A^2\Sigma^+ \rightarrow X^2\Pi$) at 5.5 eV ($\approx 2270 \text{ \AA}$). The photodissociation threshold occurs at 6.48 eV ($\approx 1930 \text{ \AA}$). Many of the measured absorption peaks in the 1700 to 2300 \AA spectral range as shown in Fig. 10 have been identified as those resulting primarily from the four (β , γ , δ and ϵ) bands. Typical mfp dimensions of these peaks at the assumed seed gas concentration are larger than 20 cm. Some of these transitions overlap with each other and thus they are not separable. The published absorption data and the radiative decay time inferred from the oscillator strength of respective transitions are summarized in Table II. In these we have sufficient information to compute the photoionization electron density in a seeded CO₂ laser mixture resulting from the single step and the two-step processes.

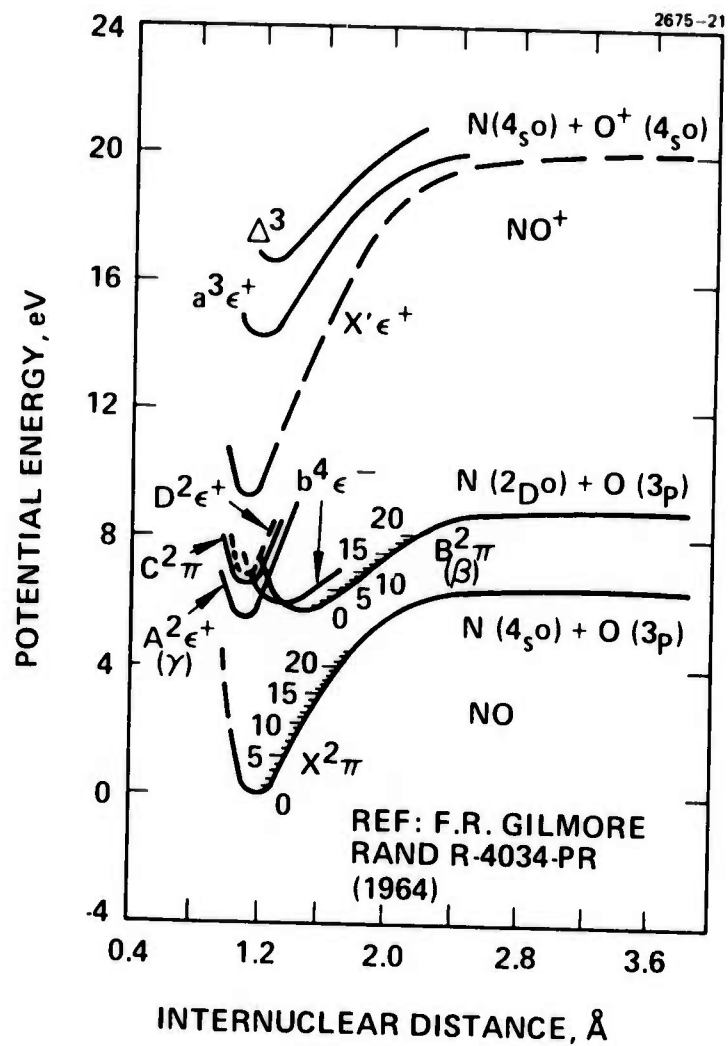


Fig. 8. Energy diagram of NO.

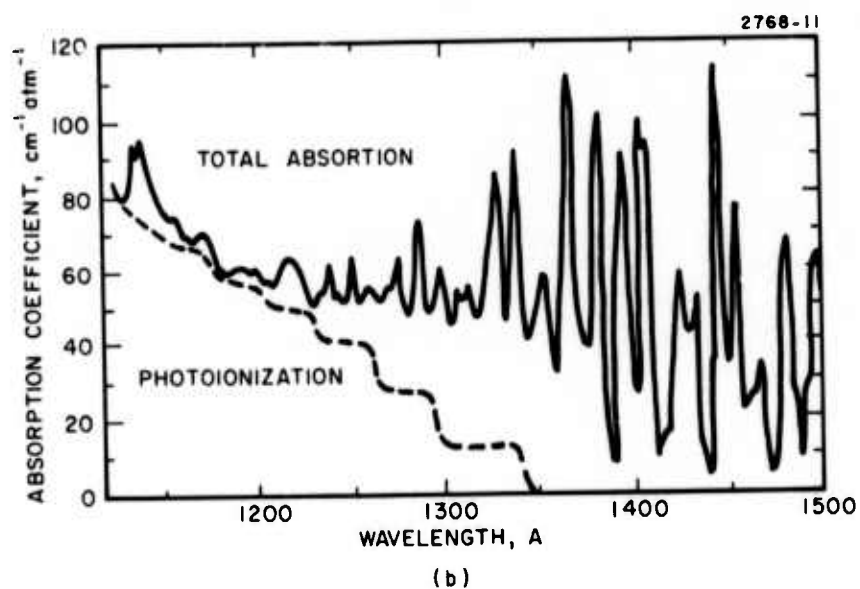
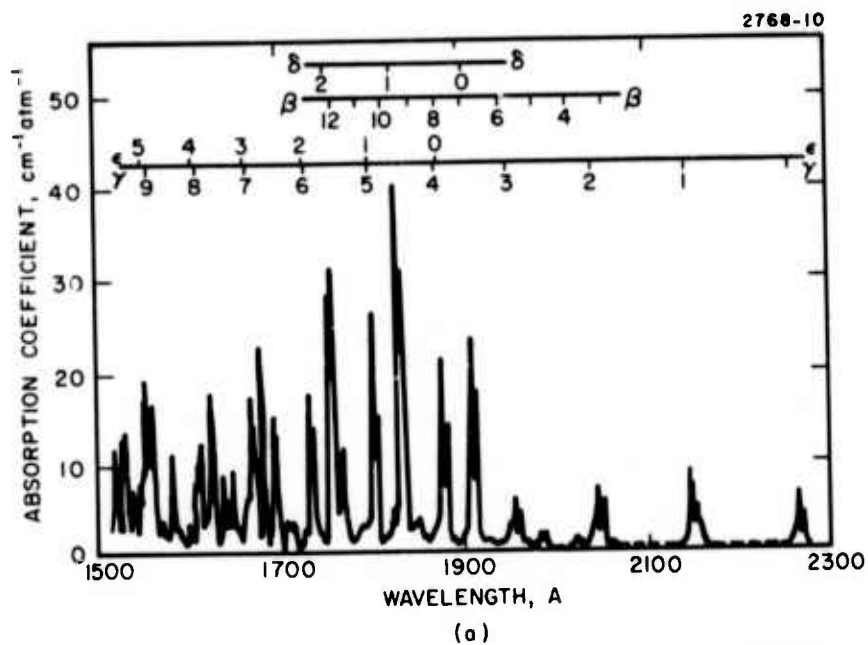


Fig. 9. The absorption spectrum of nitric oxide, NO. From K. Watanabe, J. Chem. Phys. 22, 1564 (1954).

1 atm; LASER MIXTURE; 0.5 Torr—NO PARTIAL PRESSURE

2675 24

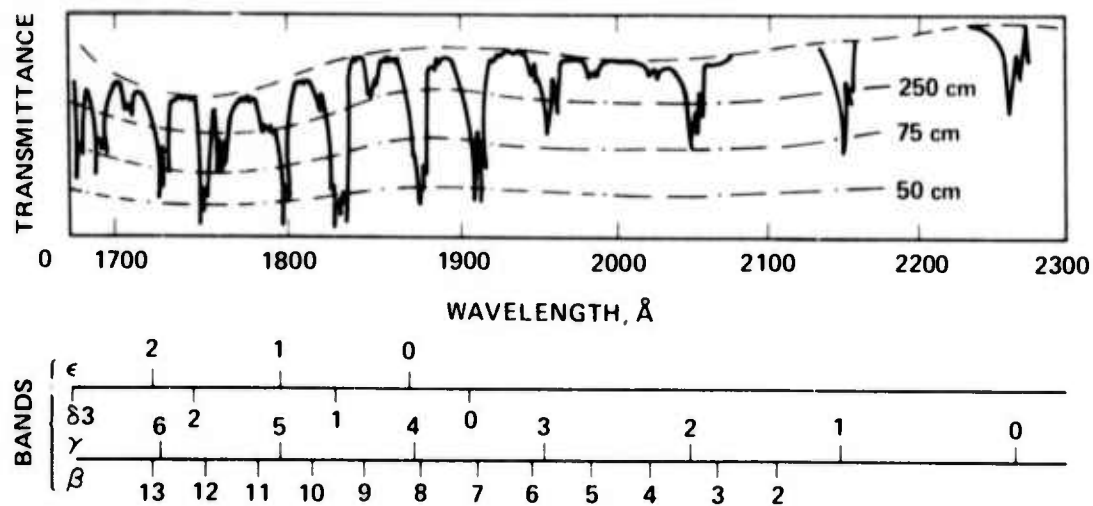


Fig. 10. Absorption spectrum of NO. From F.F. Marmo, J. Opt. Soc. Am., 43, 1186 (1953).

TABLE II

Integrated Absorption Coefficient (K_c) and Approximate
Lifetime (τ) of NO (1700 to 2300 Å)

Band (1700 to 2300 Å)	K_c^* Integrated Absorption Coefficient ($10^3 \text{ cm}^{-2} \text{ atm}^{-1}$)	τ^* Radiative Decay Time (μsec)
$\beta(2,0)$	0.037	284
$\beta(3,0)$	0.109	91
$\beta(4,0)$	0.328	30
$\beta(5,0)$	0.628	15
$\beta(6,0)$	1.10	13
$\beta(9,0)$	8.53	1.5
$\beta(11,0)$	8.62	1.3
$\beta(12,0)$	54.9	0.2
$\beta(14,0)$	4.77	2.3
$(0,0)$	9.49	1.9
$(1,0)$	18.7	0.9
$(2,0)$	16.0	0.9
$(3,0)$	8.57	1.6
$\epsilon(0,0)$ + $(4,0)$ + $\beta(8,0)$	60.4	0.2
$\epsilon(1,0)$ + $(5,0)$	109	0.11
$\delta(0,0)$ + $\beta(7,0)$	59.2	0.22
$\delta(1,0)$ + $\beta(10,0)$	137	0.09
$\delta(2,0)$	65.2	0.017
* Bethke, J. Chem. Phys. <u>31</u> , 662 (1959)		

T1112

Before we discuss the computational results, a brief mention should be made of the basic equations governing multiple excitation transitions. The two-step processes resulting from a finite number of intermediate excited states can be written in the form analogous to eq. (8) and (9):

$$\frac{d(N_1)_i}{dt} = (\sigma_0 N_0 \phi_0)_i - (\sigma_1 N_1 \phi_1)_i - \left(\frac{N_1}{\tau}\right)_i; i \leq N \quad (19)$$

$$\frac{dn_e}{dt} = \sum_{i=1}^N (\sigma_1 N_1 \phi_1)_i - \alpha n_e^2 - \beta n_e \quad (20)$$

where the subscript i refers to the i^{th} excited state. The finite total of N excited states is assumed. The first term appearing in the right-hand side of eq. (20) represents the combined production rate of photoelectrons through N separate excitation channels. The absorption data summarized in Table II are given in terms of the integrated absorption coefficient K_{oi} which is defined through an expression

$$(\sigma_0 N_0 \phi_0)_i = \int_{\Delta \epsilon} \alpha(\epsilon)_i \frac{\Delta \phi(\epsilon)}{\Delta \epsilon} d\epsilon = p_o K_{oi} \frac{\Delta \phi(\epsilon)}{\Delta \epsilon} \quad (21)$$

where

$\alpha(\epsilon)_i$ = absorption coefficient of i^{th} state

p_o = partial pressure of absorbing gas

$\frac{\Delta \phi(\epsilon)}{\Delta \epsilon}$ = photo flux density per unit increment of photon energy.

For the present illustration, we shall assume a simple UV incident spectrum as shown in Fig. 11. The shaded area represents the CO_2 absorption band. The long wavelength emission spectrum ($\lambda > 1600 \text{ \AA}$) approximates the part of flashlamp output from a high quality UV transmitting tube (i. e., suprasil). The spark UV source immersed in the CO_2 mixture basically shows the similar characteristics with a broad continuum extending from 1600 \AA to at least 3000 \AA . The spark source used without a window material gives rise to an additional spectrum in 1200 \AA passband with its amplitude much lower than that of the long wavelength region. The reduction factor δI_0 is introduced in order to account for this difference; typically this value is found to be 0.1 - 0.3.

The computed photoelectron densities (n_e) as a function of the incident UV intensity (I_0) are plotted in Fig. 12 for both the single and two step processes. The functional dependence of the attachment and recombination dominated regions as discussed in Section II-B are exhibited in this figure. At low UV intensity single step photoionization is more efficient. At the $n_e \approx 10^{12}$ electrons/ cm^3 level, two step process requires the intensity to be more than one order of magnitude larger. As the level of n_e is increased, the difference in the required UV intensities becomes smaller. At $n_e \geq 10^{13}$ electrons/ cm^3 , the two processes will require about the same level of excitation. It should be cautioned that these comparisons are at best semiquantitative. During the next period, the model will be refined and more detailed emission spectra of various sources will be incorporated into the analysis.

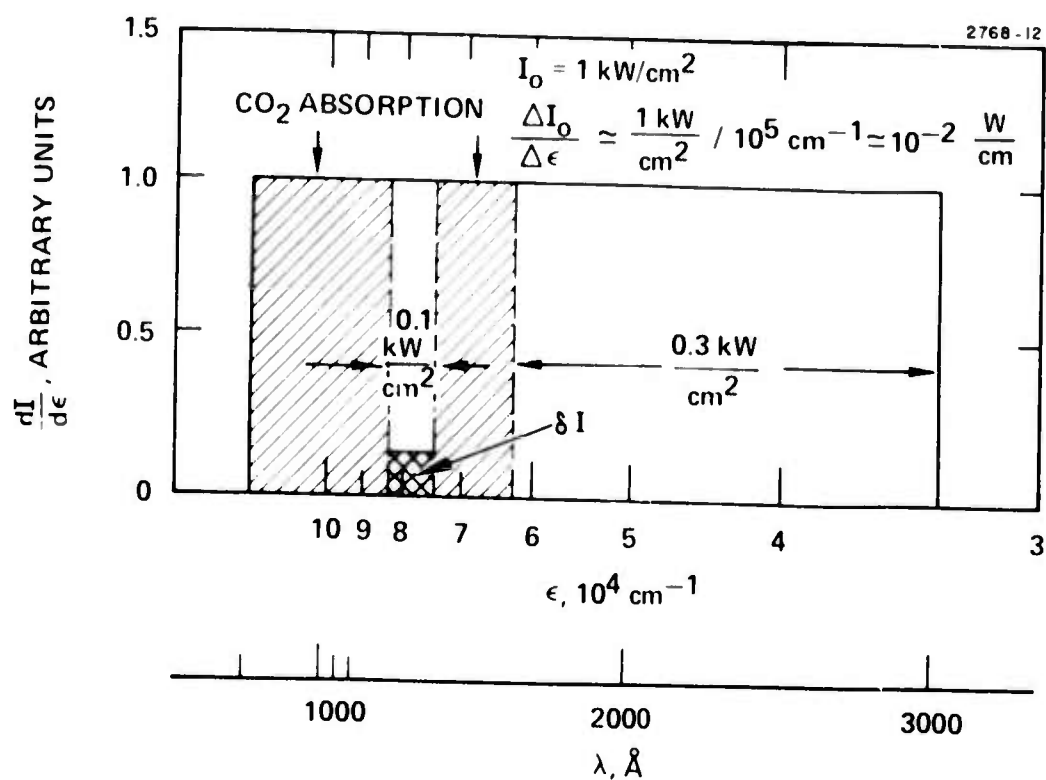


Fig. 11. Simplified emission model used for analysis.

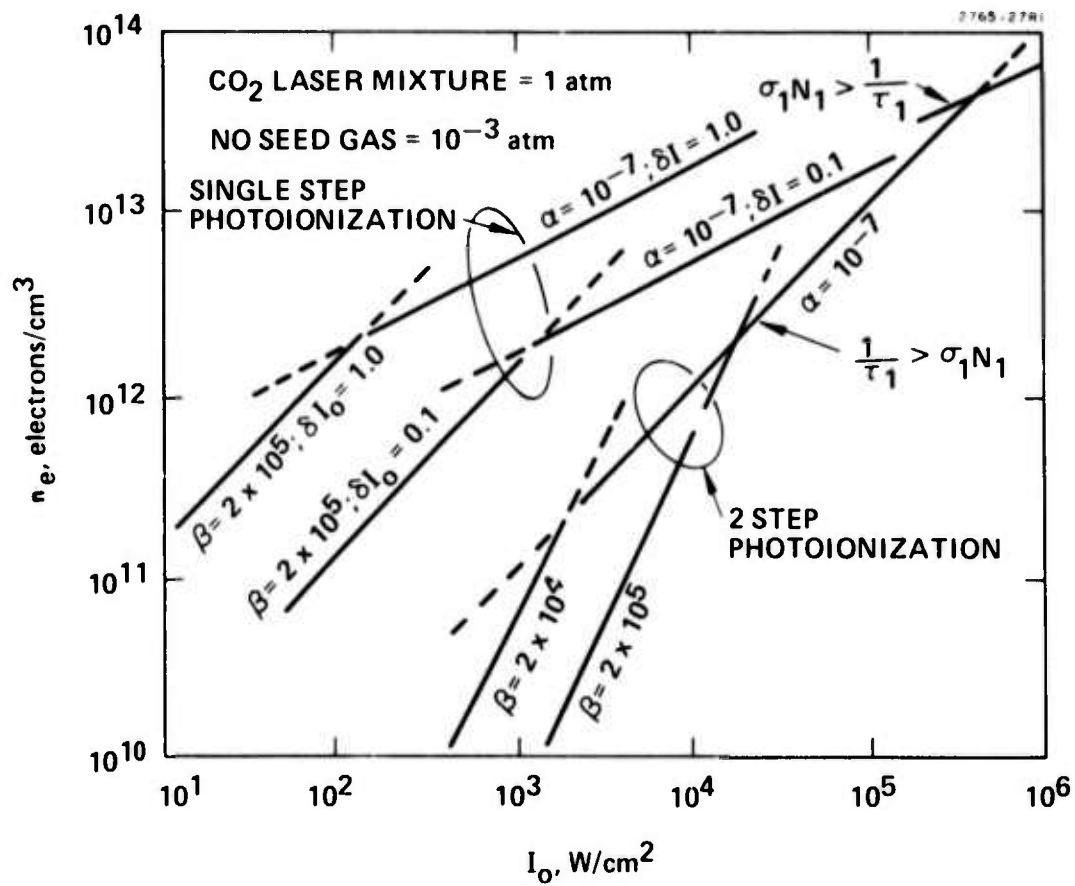


Fig. 12. Summary of photoionization in NO seeded CO₂ mixture.

III. EXPERIMENTAL PROGRAM RESULTS

A number of significant results have been obtained during the first six months of the program. These results were primarily obtained using small scale devices. The results, however, are illuminating enough to lead to realistic scalability limits that will be discussed in this section.

The results to be presented fall basically into four categories: (1) plasma discharge measurements, (2) photoionization yield measurements, (3) UV emission spectra measurements, and (4) preliminary laser measurements.

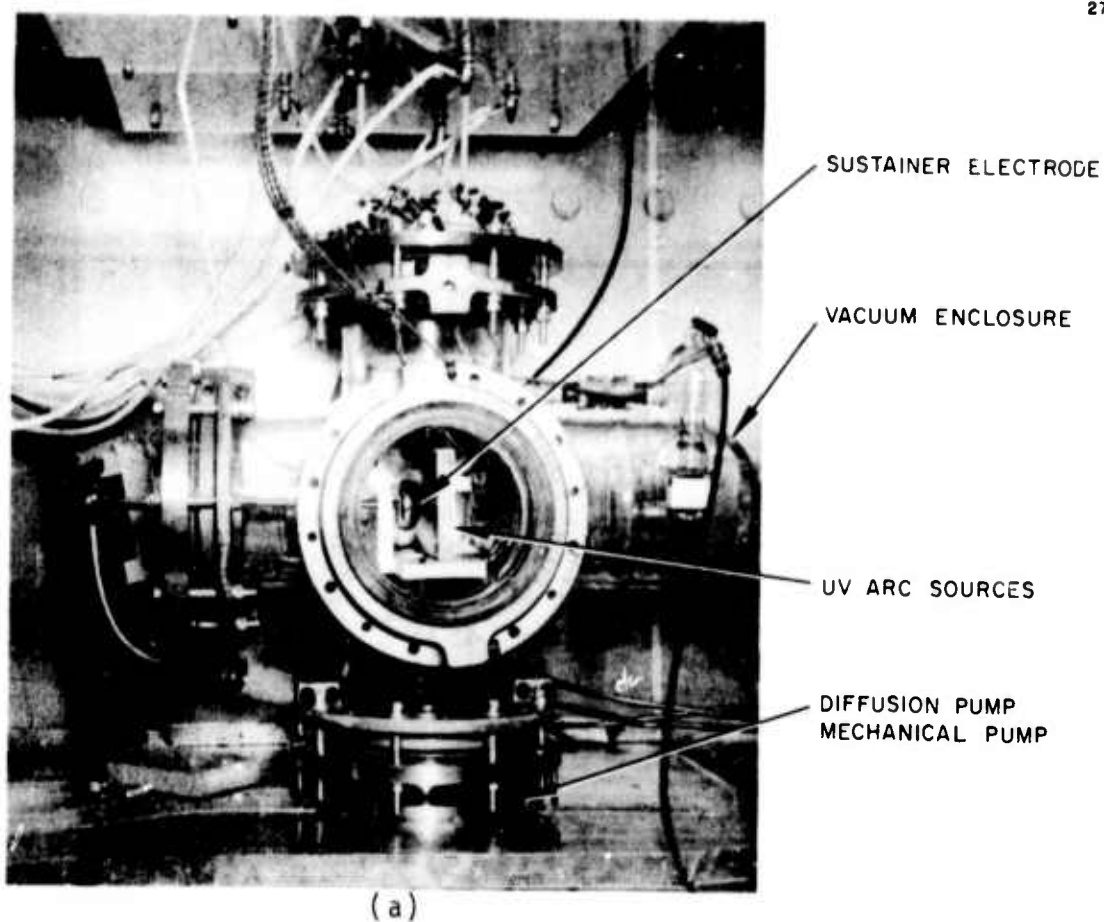
A. Plasma Discharge Measurements

1. Sustainer Energy Results

To determine the sustainer energies attainable using UV seeded plasmas parametric measurements of the current density using a small scale device, was undertaken. This device, shown in Fig. 13, consists of a Pyrex glass chamber mounted on a high vacuum station. The system is pumped to 10^{-5} Torr between each test to allow for thorough cleaning of the "sticky" organic molecules from the system. The sustainer configuration consists of a copper mesh screen, through which the UV radiation passes, and a solid stainless steel electrode. The geometry of the UV source consists of a row of sparks located adjacent to the sustainer electrodes. This geometry was initially chosen because of the need to investigate the limits of spark discharge which were located in the laser gas itself with further flashlamp type arrangements to be investigated at a later date. Figure 14 gives a diagram of the circuits employed.

For the results to be presented the seed gas used in all cases (except where noted) was Tri-n-propylamine. The ionization potential of this molecule is the lowest found, 7.23 eV, for organics. To enable the addition of a controlled amount of organic vapor a closed cycle system was employed. A hypodermic needle filled with a calibrated amount of organic liquid was inserted through a rubber septum into the device

2768-1



2768-2

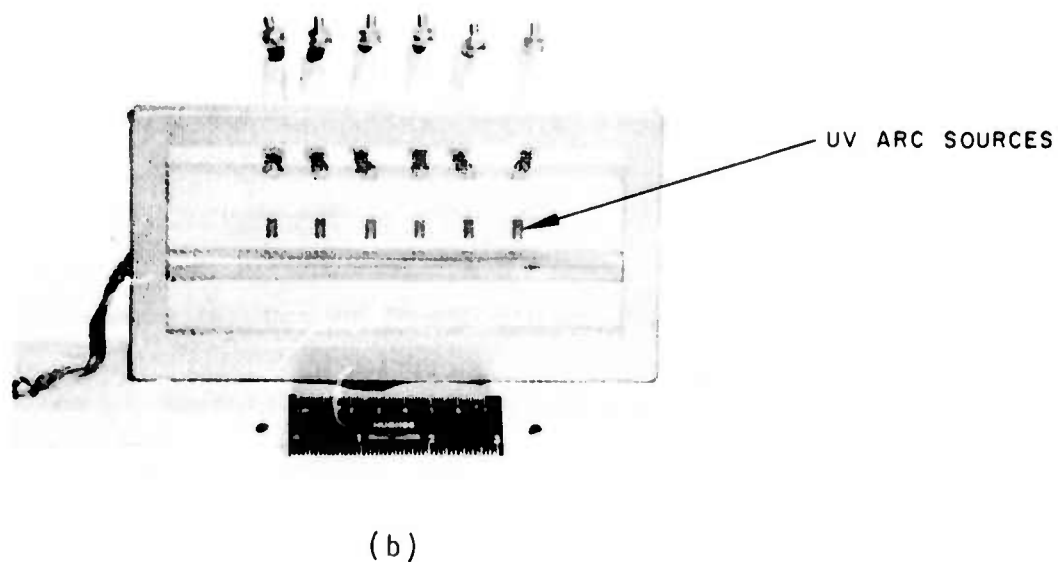


Fig. 13. Photograph of test device.

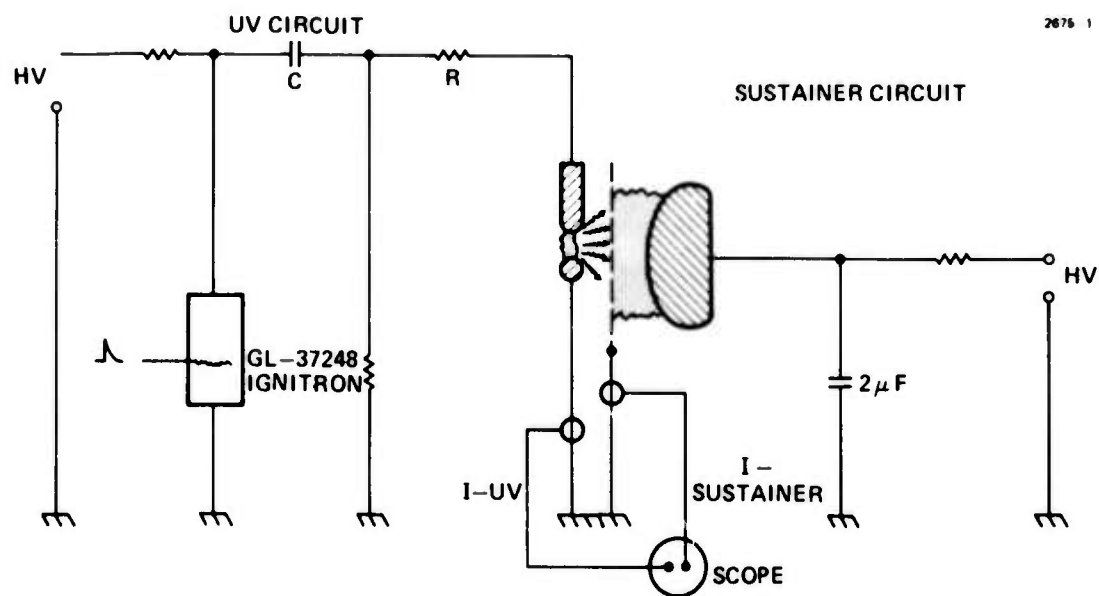


Fig. 14. Schematic of UV spark and sustainer circuits.

which was maintained under vacuum. The liquid vaporizes thereby resulting in a known partial pressure of vapor. A typical calibration curve along with a schematic of the calibration chamber is shown in Fig. 15.

To determine the current a Rogowski coil (see Fig. 14) is used. A typical oscilloscope record of the sustainer and UV currents is shown in Fig. 16. Figures 16(a) and 16(b) give the results for an overdamped and underdamped circuit respectively. (These results were obtained by changing the value of resistance R in the circuit.)

The mixture in each case was 0.02/0.3/0.675 $\text{CO}_2/\text{N}_2/\text{He}$ and the E/N of the sustainer was 4.5 kV/cm-atm, well below breakdown. These traces indicate that it is possible to produce UV sustained current pulses on the order of 50 μsec in duration. Evidenced also by the results of Fig. 16(b) is that by proper circuit design the UV source can completely control the sustainer pulse. From traces such as these the amount of energy input into the discharge was determined by direct integration

$$E_{\text{sus}} \approx V_{\text{sus}} \int_0^{t_{\text{pulse}}} I(t) \cdot dt \quad (22)$$

This procedure has been followed for a considerable number of cases with the highlights of these results to be presented in the following figures. For these figures the spark intensity, characterized by the current in the UV circuit, is the abscissa. The choice of UV current is based upon the fact that the voltage at which the arc sustains itself remains reasonably constant for the various experimental conditions employed. Thus the arc energy deposited in the gas, and consequently the radiated energy, will depend primarily upon the current. In addition, measurements of the radiated intensity using a photocell indicated a nearly linear increase in intensity with current.

In Fig. 17 we see the effect that a change of the concentration of seed gas produces on the sustainer energy. The results indicate that too low a concentration generates insufficient photoionization, and

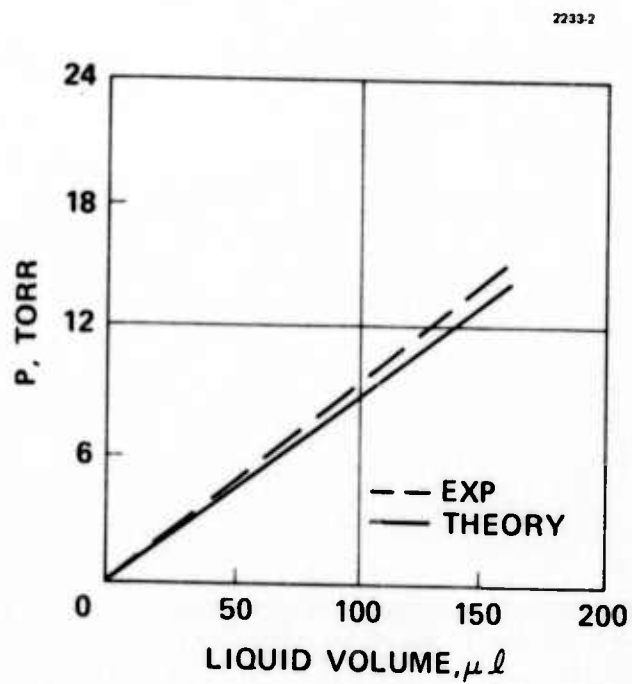
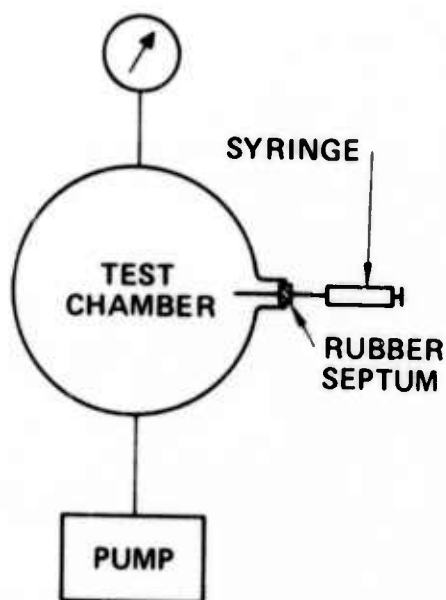


Fig. 15. Calibration curve for hypodermic syringe, and calibration.

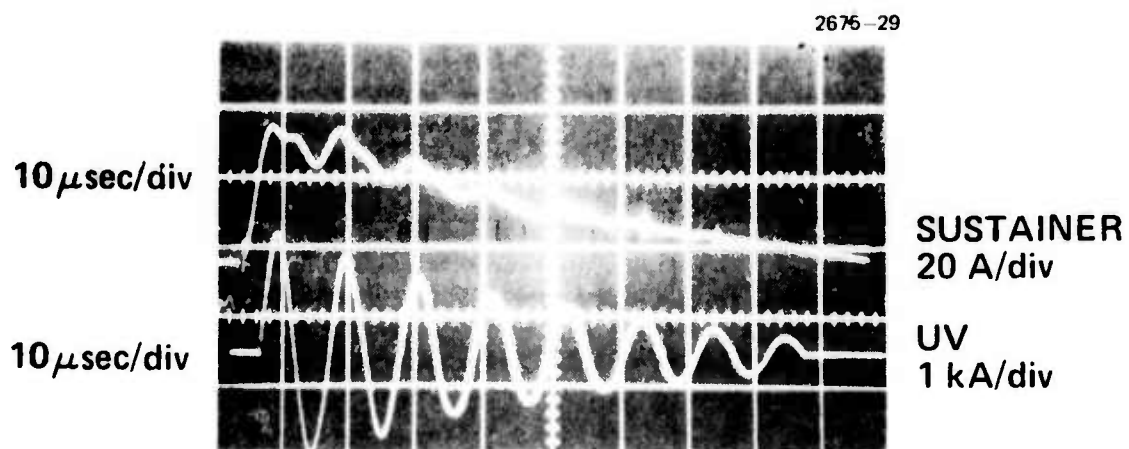
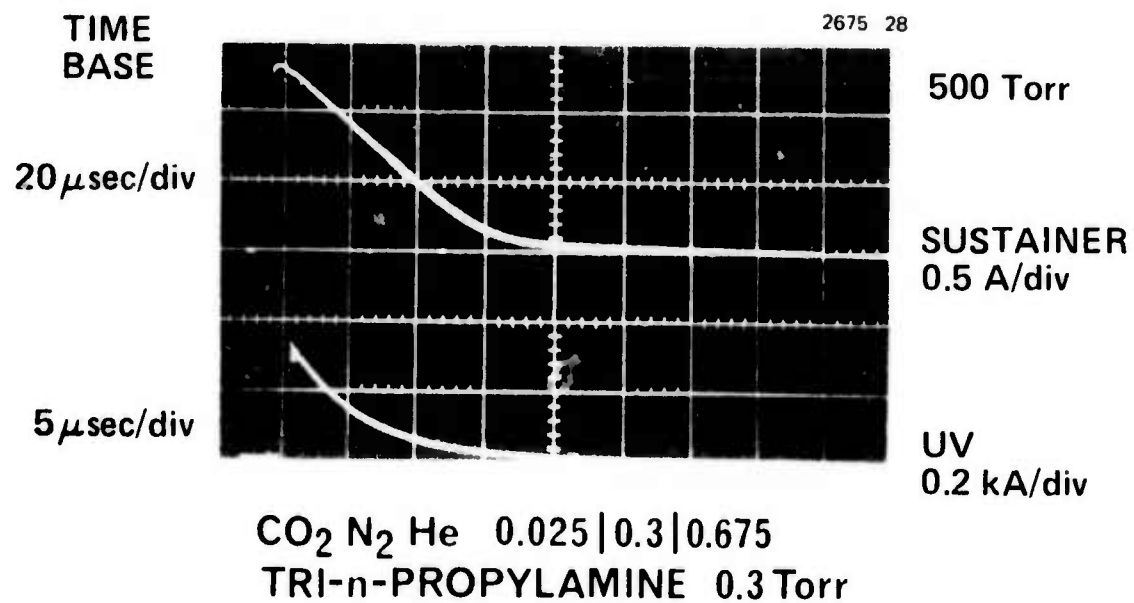


Fig. 16. Oscilloscope trace of sustainer and UV current.

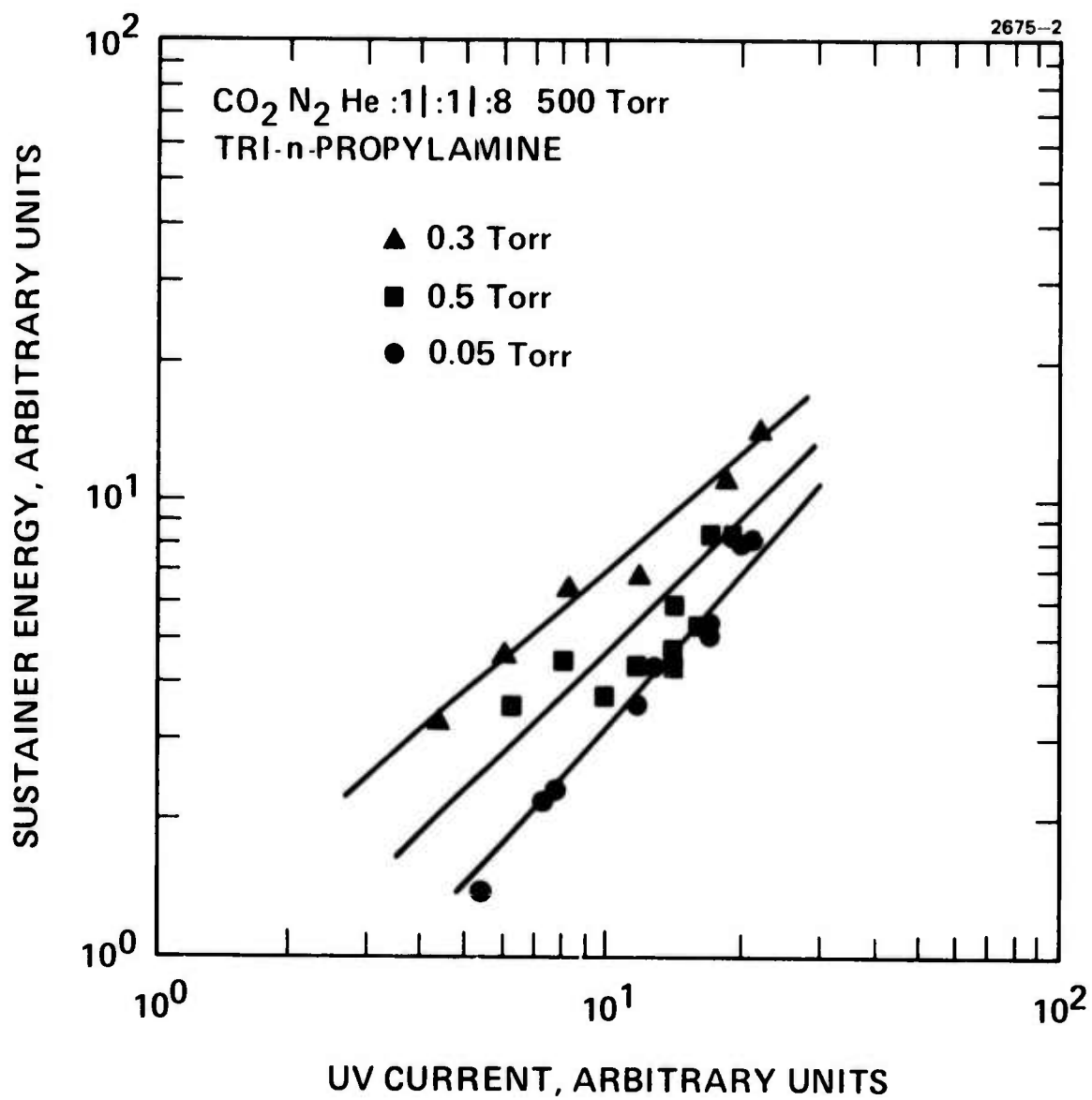


Fig. 17. Sustainer energy as a function of UV current for various concentrations of Tri-n-propylamine.

too high a concentration leads to a detrimental absorption of the UV photons thereby reducing their mean free path. Consequently, an optimum concentration is reached as evidenced by the results given in Fig. 17.

The results in Fig. 18 represent the sustainer energies achieved for tests conducted at various total pressures with a constant mixture ratio and seed gas concentration. Plotted is the relative sustainer energy normalized to the pressure as a function of the relative UV current. The results indicate, to within the experimental error (approximately 20%), a universal curve for all pressures. Thus one concludes that the sustainer energy scales linearly with pressure. This statement is clearly not correct, however, if the mean free path of the mixture decreases with increasing pressure. This will be discussed further below.

Figure 19 illustrates the relative sustainer energy for four CO₂ laser mixtures at constant total pressure and fixed seed gas concentration. The results show that a lowering of the CO₂ concentration generally leads to increased sustainer energies. One can see, however, that the results for the 0.01 and the 0.025 CO₂ mixtures are essentially identical. These two facts support the conclusion that the effective mean free path of the mixture is dominated by the CO₂ concentration. Consequently for the low CO₂ mixtures the mean free path must have become comparable in magnitude to the UV spark-sustainer electrode spacing. For the present geometry this corresponds to a distance of approximately 4 cm. This can qualitatively be understood by writing an expression for the sustainer energy as a function of mean free path as follows. The photon flux Φ that reaches a position z is proportional to (see eq. 1)

$$\Phi \propto \frac{e^{-z/\lambda_{\text{mix}}}}{z^\gamma} \quad (23)$$

where λ_{mix} = mean free path of mixture

$\gamma = 0, 1, 2$ for a planar, line or point source.

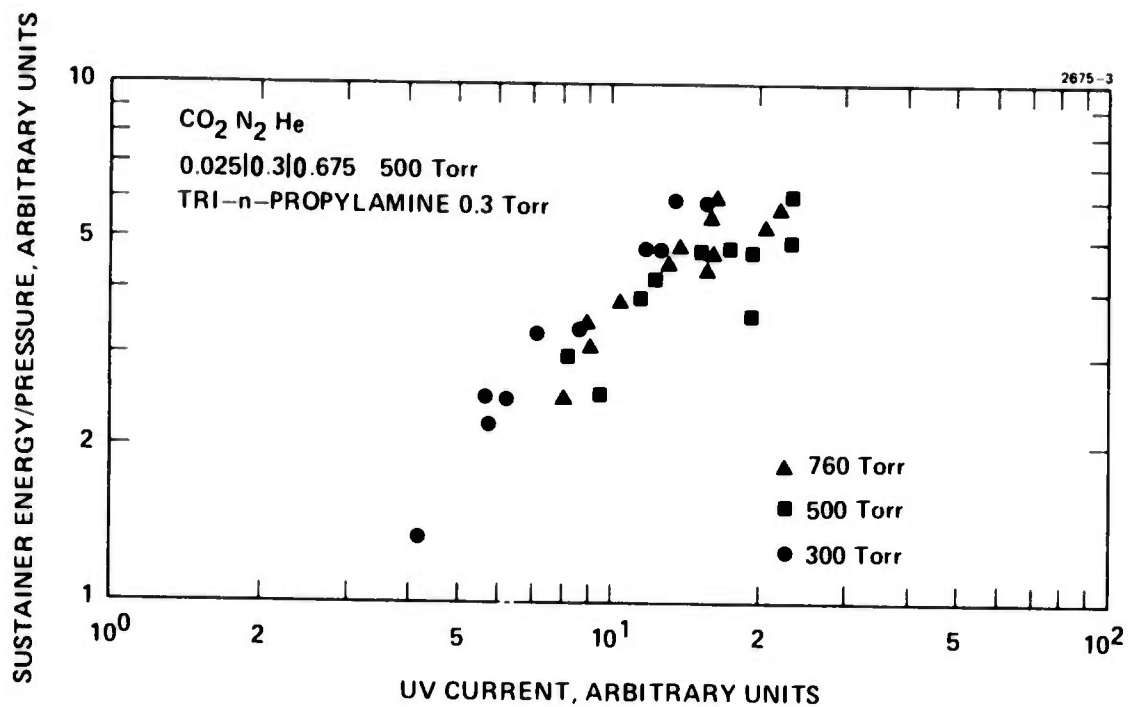


Fig. 18. Sustainer energy normalized to total pressure as a function of UV current for various total pressures.

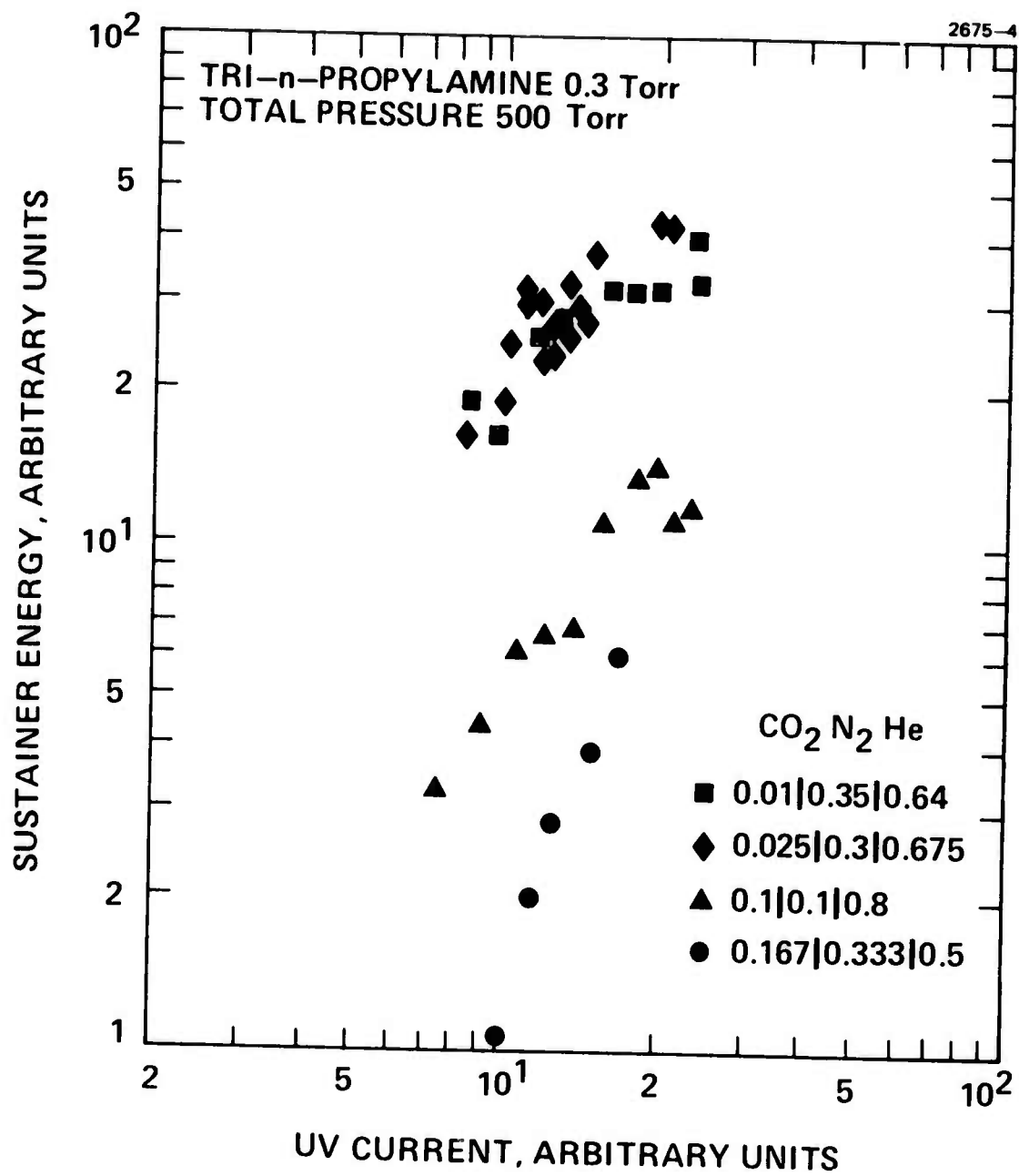


Fig. 19. Sustainer energy as a function of UV current for various laser mixtures.

The number of electrons $S(n, z)$ produced per second by photoionization is (see eq. 2)

$$S(\nu, z) = \sigma_s(\nu) n_s \Phi(\nu, z) \quad (24)$$

where $\sigma(\nu)$ is the seed gas photoionization cross section and n_s is the seed gas number density. Now assume, for this argument that a steady state electron number density is produced in the discharge established by recombination balancing photoionization. The electron number density will consequently be proportional to $S^{1/2}$ (see Table I),

$$n_e \propto S^{1/2} . \quad (25)$$

Thus, inserting (23), (24) and (25) into (22) we obtain

$$E_{\text{sus}} \propto \frac{1}{\lambda_s} e^{-z/2\lambda_{\text{mix}}} \quad (26)$$

where

$$\lambda_s = \frac{1}{\sigma_s n_s} .$$

Rewriting for the ratio of two mixtures gives

$$\frac{E_{\text{sus}_i}}{E_{\text{sus}_o}} = \left(\frac{\lambda_{s_o}}{\lambda_{s_i}} \right)^{1/2} e^{z/2\lambda_{\text{mix}_o}} \left(1 - \frac{\lambda_{\text{mix}_o}}{\lambda_{\text{mix}_i}} \right) \quad (27)$$

Forming this ratio from the data of Fig. 19 and comparing with that calculated from eq. (27) we have the following:

	$E_{\text{sus}_i} / E_{\text{sus}_o}$	
X_{CO_2}	Exp	Equation (27)
0.167	1	1
0.1	2	2.5
0.025	8	7.1
0.01	8	8.6

These results give the qualitative trends expected. In eq. (27) λ_{mix} was a free parameter which when adjusted gave the values shown. The λ_{mix} determined in this manner was 6 cm for the 0.025 CO_2 mixture. This will be shown later (see Fig. 27) to be in close agreement with the mean free path expected based on the spectral characteristics of the radiation.

Referring again to the discussion following Fig. 18 we can now understand why the sustainer energy scaled with the total pressure — because these tests were in fact performed with the 0.025 CO_2 mixture. Further understanding of this results from additional tests performed using 0.1/0.1/0.8 mixtures at various total pressures. These tests gave results indicating an increase in signal with decrease in pressure in agreement with the above arguments.

In addition to the above parametric variations, changes in the UV circuit parameters were also studied. The objective of these tests was to determine the important circuit scaling parameter for the UV source. A variation of the resistor R (see Fig. 14) or of C and the applied voltage (i. e., stored UV energy $1/2 CV^2$) was performed. The results are given in Fig. 20 where the sustainer energy is plotted as a function of the current through the UV spark circuit. The data obtained correlate to the UV current indicating this to be, as discussed from the outset, the important scaling parameter for the spark.

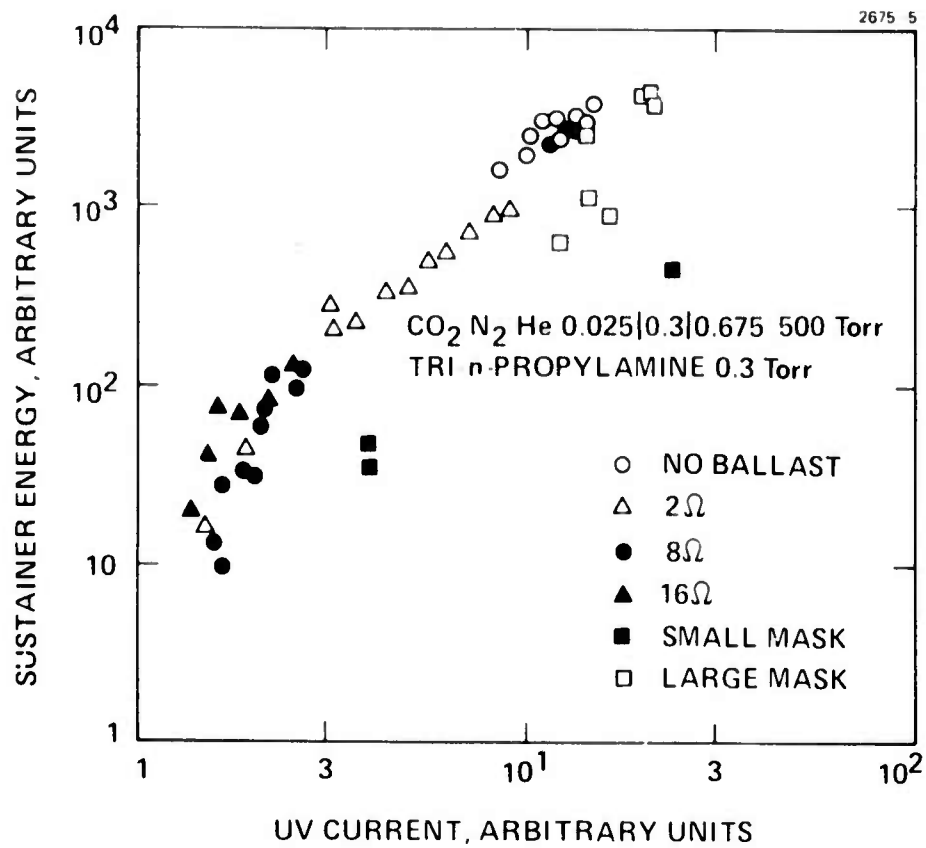


Fig. 20. Sustainer energy as a function of UV current for various ballast resistances.

2. V-I Characteristics

A further test performed related to a determination of the V-I characteristics of the discharge. The results of one such run are shown in Fig. 21. The data indicate (solid line) a linear variation as is expected for operation of the discharge below avalanche conditions. The straight line, however, does not pass through the origin. To explain this required a series of separate experiments since it was not possible to obtain data below that shown on the solid line due to signal-to-noise problems. These experiments employed a single spark chamber (to be discussed in part III-B) and a Faraday cage to measure the current produced. From such experiments it was determined that the curve in fact originates as the dotted line in Fig. 21. The dotted line represents the V-I characteristics of the cathode sheath. At a certain sheath breakdown voltage, V_{susmin} , the charge carriers produced by the photoionization of the Tri-n-propylamine carry the current throughout the gap with the sheath collapsing to a size similar to that present in a glow discharge. As the voltage is increased a linear increase (ohmic region) in current is obtained until the value of V_{susmax} , defined as the voltage at which avalanching in the seed gas occurs, is reached. These voltages V_{susmin} and V_{susmax} thus define the operating range of UV sustained discharges.

3. Discharge Volume Determination

With the parametric variation of the sustainer energy now well documented, it is of interest to determine the energy density that is input to the discharge. To achieve this the plasma volume must be determined. For the present experiments this was accomplished through the use of a teflon mask inserted between the sustainer electrodes with a known area removed. Two such masks were made, one with twice the open area of the other. The results from the tests using these masks are shown on Fig. 20 as the large boxes. These energy results when divided by the now known plasma volume indicate a substantial decrease in energy density from that obtained with no masks. Such a result implies that for the mask sizes used, relative to the flat and

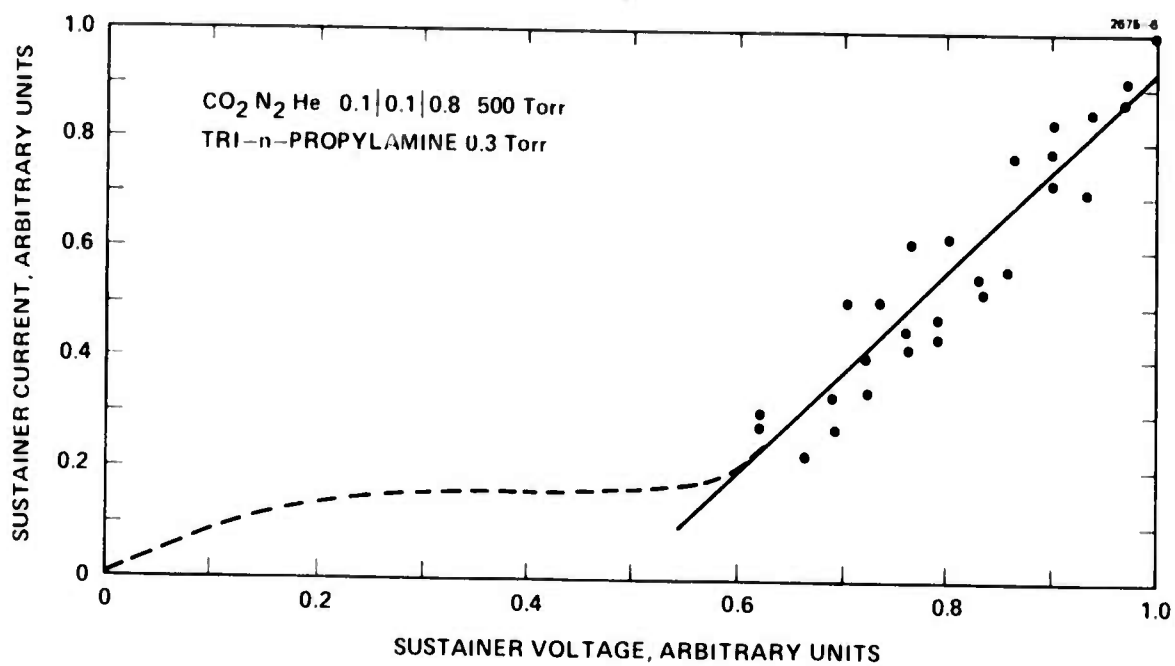


Fig. 21. V-I characteristics of the plasma discharge.

curved portion of the electrode, the curved portion contributes substantially to the current obtained. This is somewhat plausible based on the fact that even though the E field is much smaller in the curved region, the electrons in that region (produced by the volume photoionization) contribute in a linear manner to the measured current. Whereas for avalanche conditions, the larger E field region dominates the electron production due to the exponential growth rate dependence on E of the electrons in that region. In any event, from the energy measurement obtained with this mask inserted and utilizing the mixture which resulted in the largest relative energy* (see Fig. 19), we have to date achieved an input loading in excess of 200 J/l-atm.

4. Electron Number Density Determination

Based on the current density measurements made with the masks in place, the electron number density achieved in the discharge was determined. The results based on the assumption of photoionization balancing recombination are given in Fig. 22. Shown also is a calculation of the electron number density based on the collisional ionization of the Tri-n-propylamine assuming a Boltzmann distribution of electrons in the discharge. Calculations of the contributions from the collisional ionization of CO_2 , N_2 and He were also made with number densities orders of magnitude below that achieved in the Tri-n-propylamine obtained. These calculations offer further substantiation of the fact that the discharges are indeed operating in a non-avalanche UV sustained mode.

*HRL CO_2 kinetic code preliminary results indicate that lower CO_2 concentration does not result in decreased laser output energy over levels achievable with higher CO_2 concentrations. This statement is valid provided that the N_2 concentration is increased proportionally such that $X_{\text{CO}_2} + X_{\text{N}_2}$ remains constant, and the losses in the system are below that of the now smaller gain.

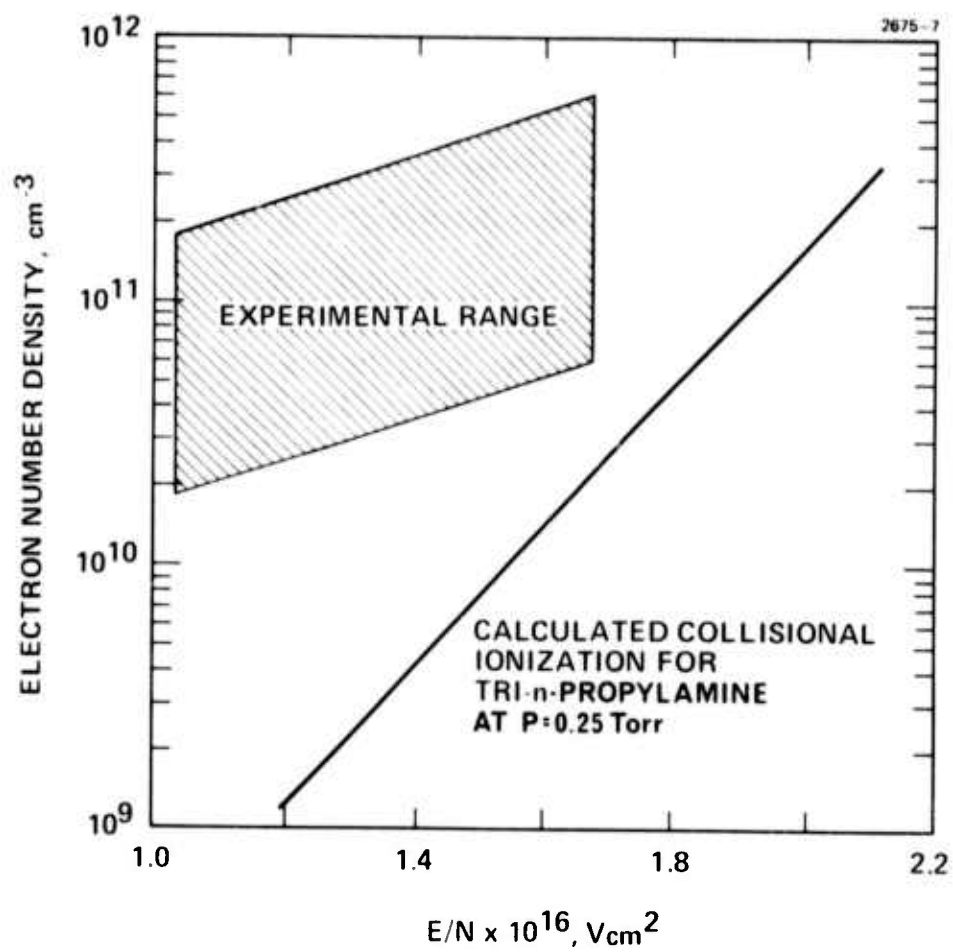


Fig. 22. Electron number density as a function of E/N .

5. Photodissociation and Contamination Results

In addition to the beneficial effects associated with the use of seed gases, certain detrimental effects are also present. As a first step in judging whether or not these detrimental effects are severe led to a preliminary investigation of photodissociation of the seeded gas. The photodissociation occurs in these experiments as a natural consequence of the use of spark discharges which are not isolated from the seed gas by a glass envelope. Consequently, the wavelengths needed for photodissociation as well as those needed for photionization are present.

To provide initial determinations of this effect the sustainer energy was measured as a function of number of discharge firings at various UV energies, seed gas concentrations and gas mixtures. Figure 23 shows the results of one such test. It can be seen that a substantial drop in sustainer energy is obtained as the number of firings increases. This result implies that a replenishment of the seed gas would be required to maintain a constant level of sustainer energy. Consequently, for single-shot operation closed cycle systems would seem feasible, however for multiple shots open-cycle systems would be needed.

For either type of system an evaluation of the contamination effects produced by the photodissociation must also be considered. Such an evaluation, limited to visual observation of the electrode surfaces, indicates that a carbon deposit is formed. However, after nearly 3000 firings the sustainer energy results obtained are repeatable, to within the experimental error, with the results obtained on the first shots. The effects on optical surfaces have not been investigated at this time.

Additional questions as to the effects of the seed gas on CO_2 laser kinetics have also been addressed. Studies of laser output obtained with a CO_2 cw laser and a pulsed CO_2 UV preionized laser, operating in the avalanche mode, indicated that for the concentrations of seed gases required for optimum photoionization no detrimental effect is observed.

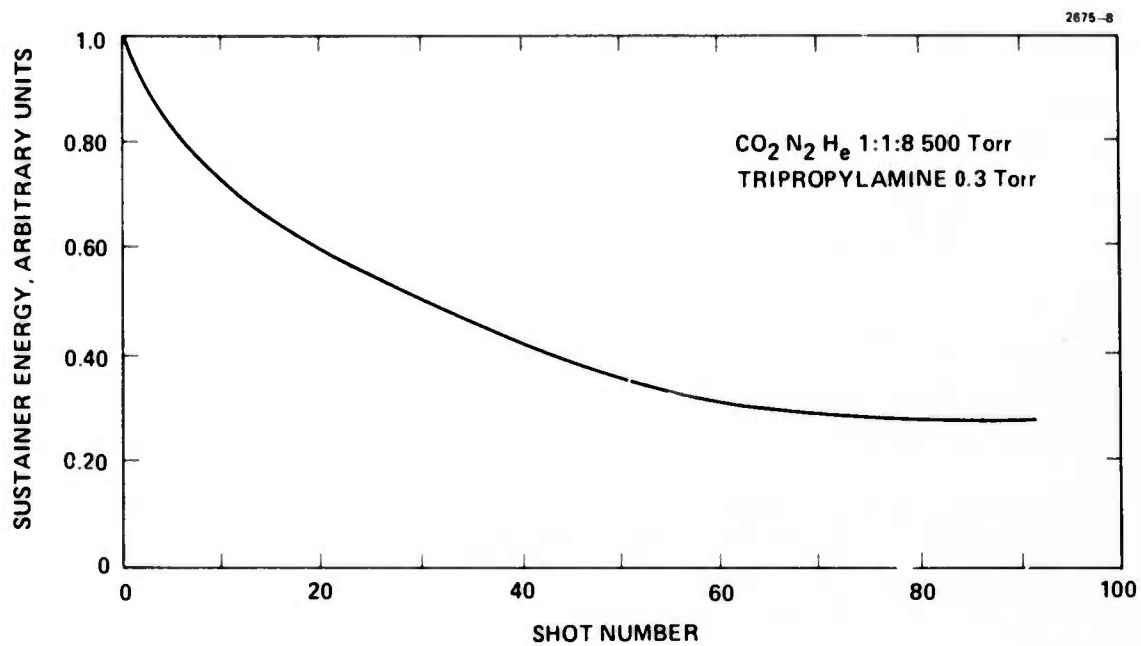


Fig. 23. Sustainer energy as a function of number of discharge firings.

B. Photoionization Yield Measurements

An effort to characterize the wavelengths responsible for producing the observed photoionization of the added seed gases was undertaken. A small photoionization chamber in which the combined seed gas and laser mixture could be separated from the spark emission chamber (see Fig. 24) was employed. The experiment was conducted by inserting several UV wavelength cutoff windows into the chamber and measuring the current drawn, using the Faraday cage, for the various wavelength bands obtained. To determine the cutoff wavelengths accurately the transmittance characteristics of each window employed was first tested on a McPherson spectrometer (see Fig. 29). The results of these tests are shown in Fig. 25.

The relative photoionization yield for the wavelength bands determined by these windows was measured for Tri-n-propylamine (ionization potential of 1720 \AA) added to a $\text{CO}_2/\text{N}_2/\text{He}$ mixture with the results given in Fig. 26. These results display the fact that the photoionization which yields the observed sustainer currents of the previous section is due to radiation with wavelengths between approximately 1200 and 1600 \AA . * One then concludes that apparently single-step photoionization is the responsible mechanism for these experiments.

The scalability limit of this single-step ionization process is determined basically by the UV photon mean free path of CO_2 and Tri-n-propylamine in the $\text{CO}_2/\text{N}_2/\text{He}$ mixture. Figure 27 gives the mean free path for CO_2 at 0.02 atm and Fig. 28 gives a rough measure of the mean free path of Tri-n-propylamine at 0.3 Torr determined from absorption coefficient measurements using the McPherson spectrometer. For such partial pressures in the wavelength range of interest it is believed that a 10 to 20 cm mean free path is a realistic value that one atmosphere CO_2 lasers can achieve.

To scale beyond these 10 to 20 cm sizes requires making use of wavelengths ($>1600 \text{ \AA}$) for which the mean free path of the constituent

*The relative percent breakdown between the wavelength regions shown is subject to as much as a 20% error due to the poor cut-off characteristics of sapphire.

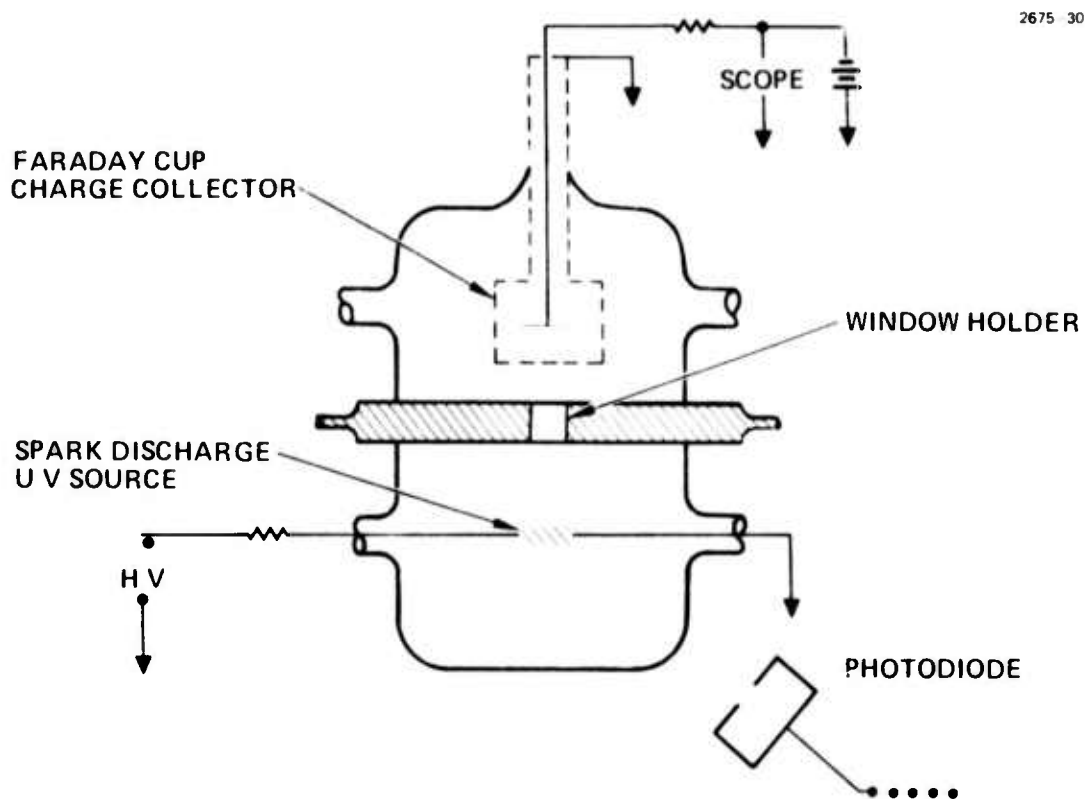


Fig. 24. Photoionization yield test chamber.

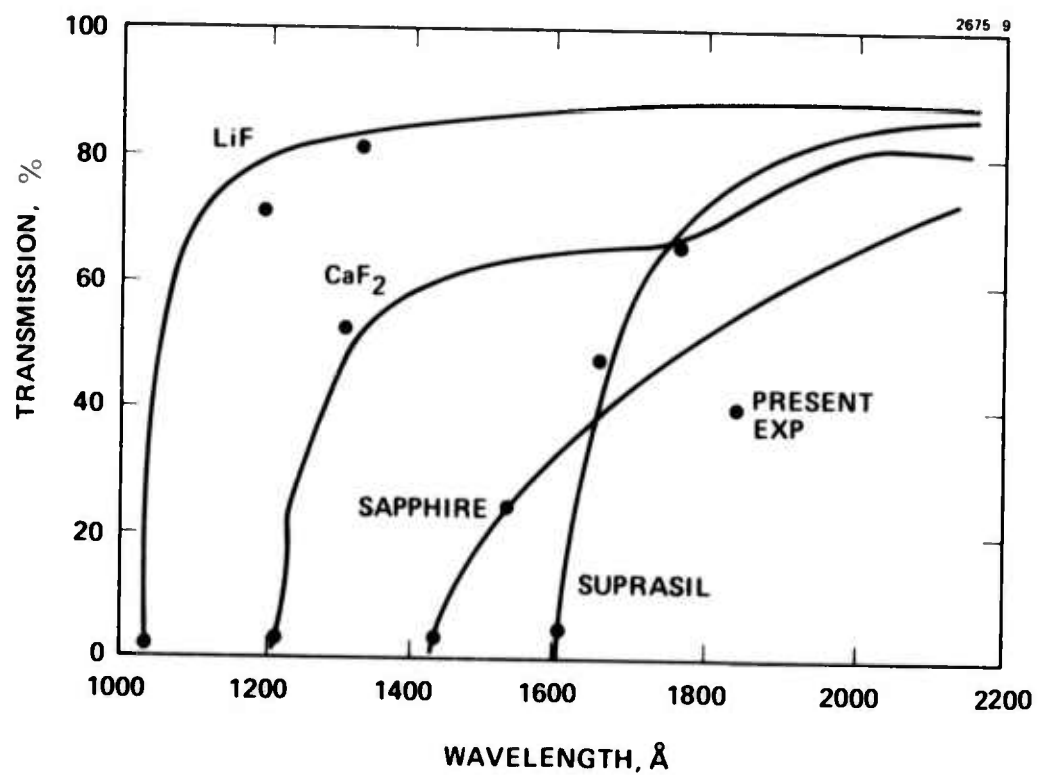


Fig. 25. UV window transmission characteristics.

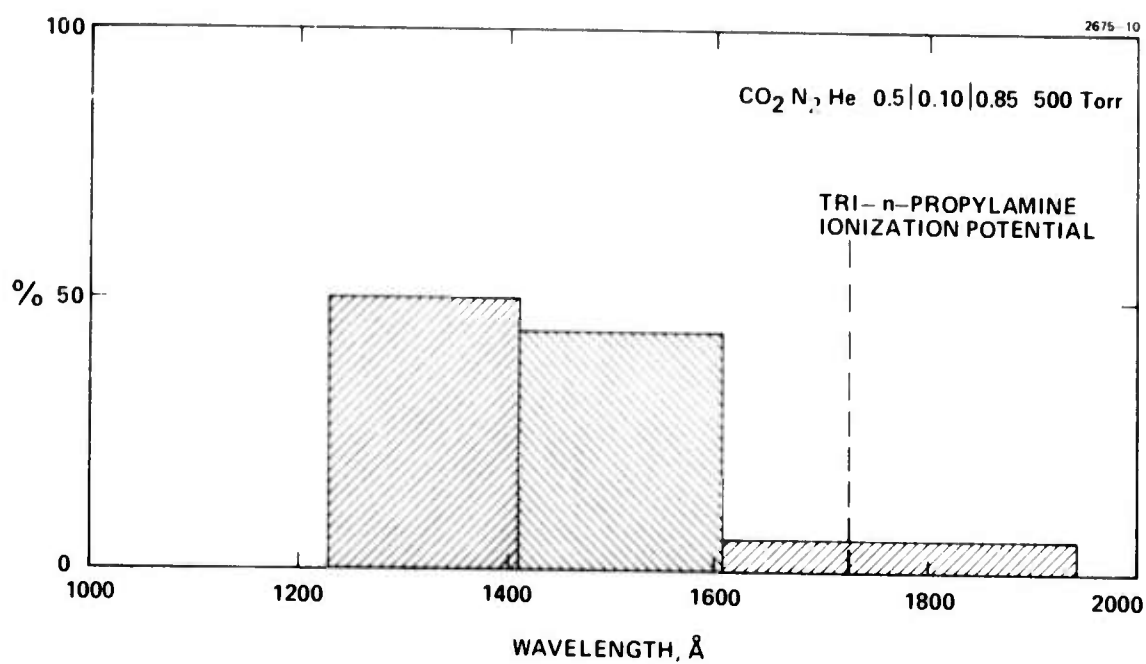


Fig. 26. Relative photoionization contribution from various wavelength regions for tri-n-propylamine.

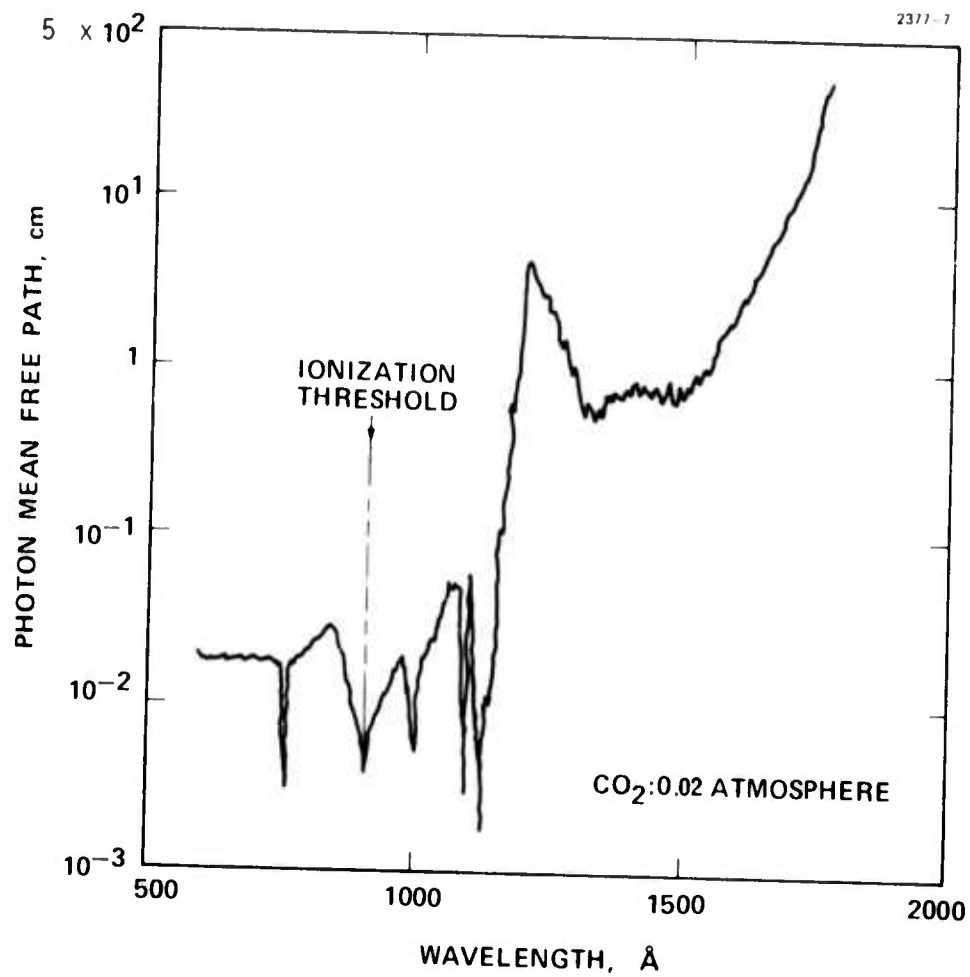


Fig. 27. UV photon mean free path through CO₂ at 0.02 atm.

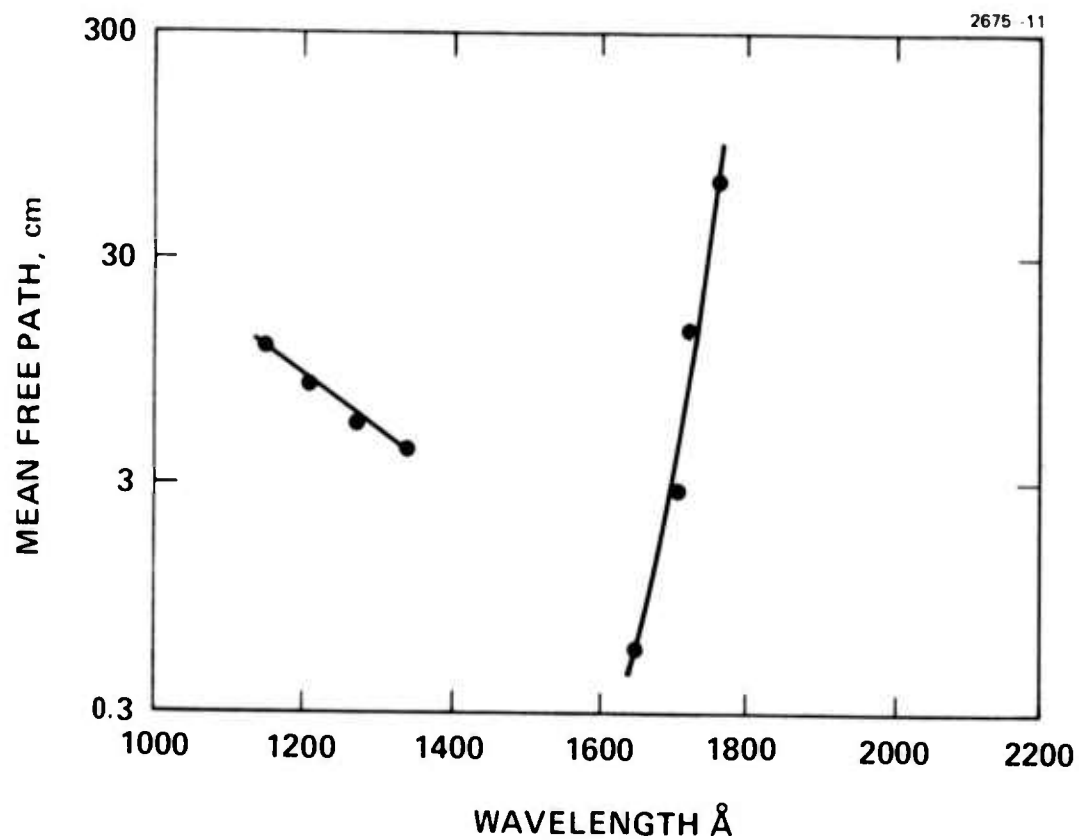


Fig. 28. UV mean free path through tri-n-propylamine at 0.3 torr.

gases is longer. Based on the mean free path data from above multi-step photoionization processes should be scalable up to the 50 to 100 cm size. This approach, however, as shown in Section II requires considerably higher UV intensities. Such high intensities can be achieved with flashlamps and an investigation to determine their effectiveness and to optimize their spectral characteristics is currently in progress.

C. UV Emission Spectra

In conjunction with absorption measurements and photoionization yield measurements a knowledge of the emission spectra of the spark sources used in the present experiments is a critical element. A program to investigate their emission spectra was consequently undertaken. The experimental configuration is shown in Fig. 29. The spark source is placed as close to the McPherson spectrometer entrance slit as practical (approximately 2-3 cm). Based on the results of the previous section, which indicated that the wavelength region of interest spans the range from 1200 Å and longer, a LiF window (cutoff at 1050 Å) was used to isolate the spark source from the spectrometer.

Figure 30 displays the effect of varying the UV current through the spark for a He discharge. Three currents of 300, 400 and 550 A are shown. (Due to experimental limitations 550 A was the peak current that could be achieved.) It is apparent that increased current leads to increased emission with no apparent change in the relative spectra.

In Fig. 31 the emission spectra of N₂ at a current level of 300 A is shown. The comparable He spectra is also given. Note that the N₂ and He spectra are similar but the N₂ intensity is substantially increased. The similarity is due to the fact that most of the lines observed in the He data arise from the small level of N₂ impurity in the He. Many of these observed lines can be attributed to atomic nitrogen spectra.

Several electrode materials were investigated with no appreciable difference in their spectra. Since the current levels are below that expected to yield metal vapor spectra, this is not unexpected.

A final spectra measured was that of the laser gas mixture. Two mixtures were studied with concentration of CO₂/N₂/He of

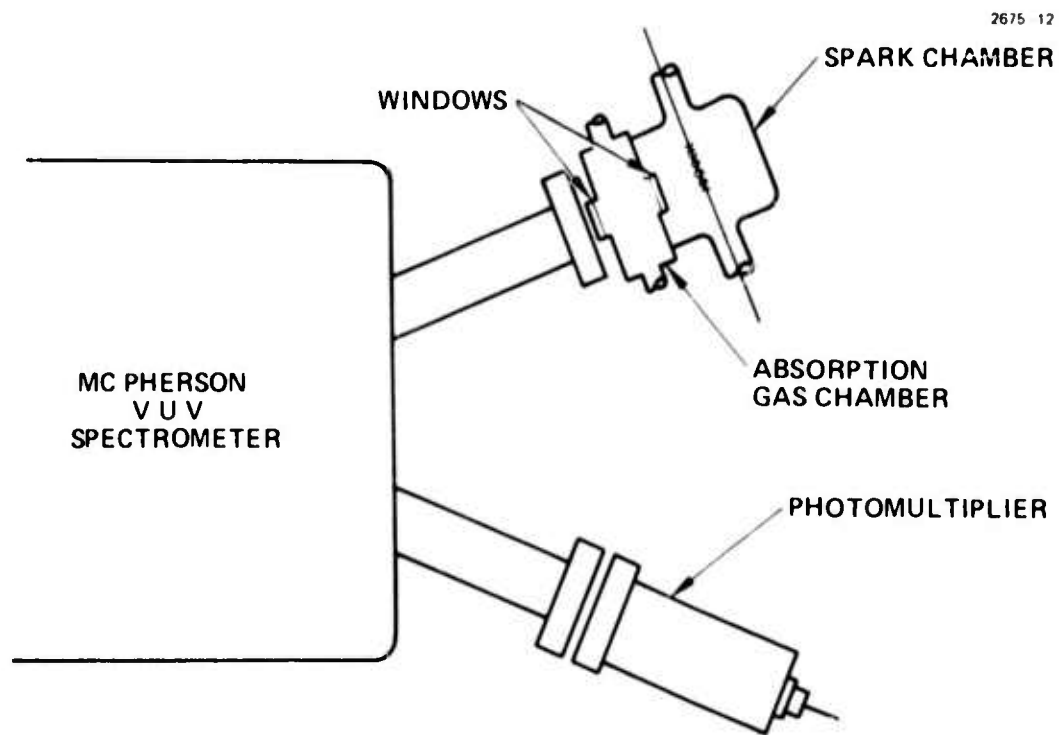


Fig. 29. Test setup for spark spectrum emission and absorption measurements.

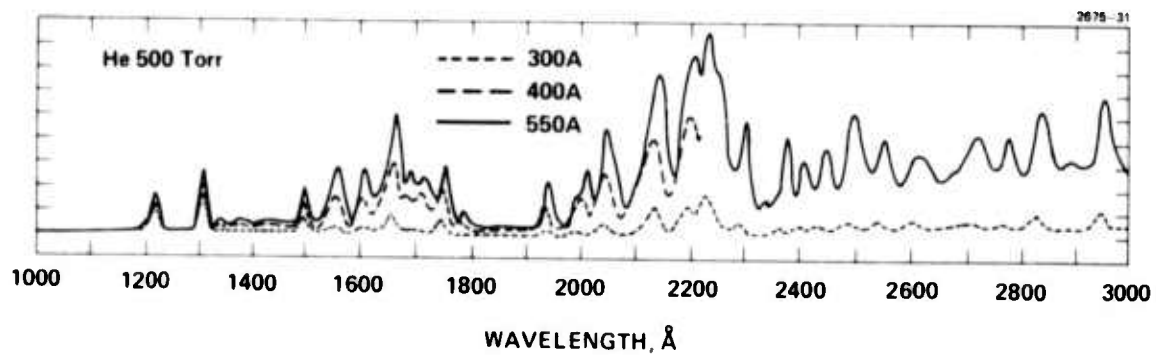


Fig. 30. Relative emission spectra of a He spark discharge for three current levels.

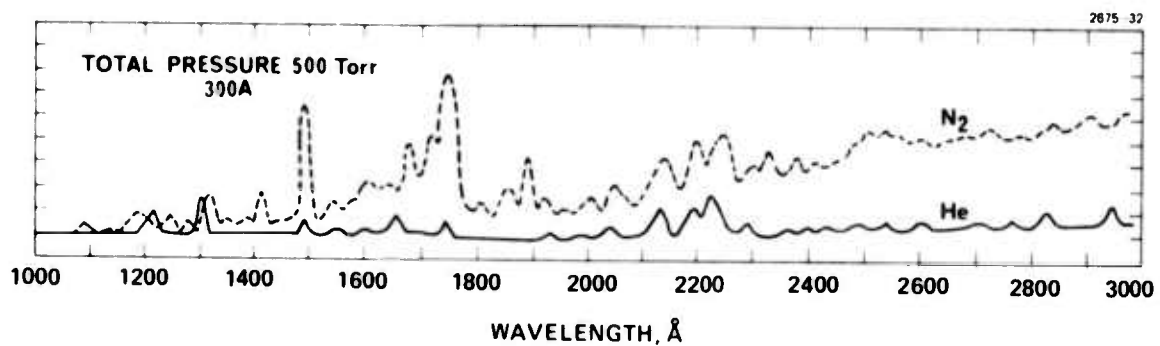


Fig. 31. Relative emission spectra of N₂ and He at 300 amps.

0.5/0.10/0.85 and 0.025/0.3/0.675. The emission spectra, which of course, in this case is combined emission-absorption spectra, for these mixtures is given in Fig. 32. It is apparent from these spectra, at these current levels, little radiation below 1600 \AA passes through the gas as would be expected based on the mean free path data for CO_2 .

To qualitatively demonstrate what affect the change in spectra observed in the above figures would have on the photoionization of Tri-n-propylamine photoionization yield measurements were made. For these tests the emission chamber was isolated from the photoionization chamber by a LiF window (see Fig. 24). The emission chamber was filled with either He, N_2 , or a 0.5/0.10/0.85. $\text{CO}_2/\text{N}_2/\text{He}$ mix with the photoionization chamber filled with a 0.5/0.10/0.85 mix and Tri-n-propylamine. The sustainer energy results, shown in Fig. 33, illustrate the expected increase using N_2 as the emission gas. They do not however show an increase with He as might be expected based on the emission spectra.

D. Preliminary Small Signal Gain Measurements

The primary goal of the work to date dealt with an understanding of the physical mechanisms taking place in UV sustained plasmas. Consequently no laser output data was obtained. A preliminary measurement of small signal gain, however, was made. These results (see Fig. 34) are for a benzene seeded mixture. Also shown in the figure are calculated results from the HRL CO_2 kinetic for 20 and 40 μsec pulse lengths. The agreement is seen to be fair.

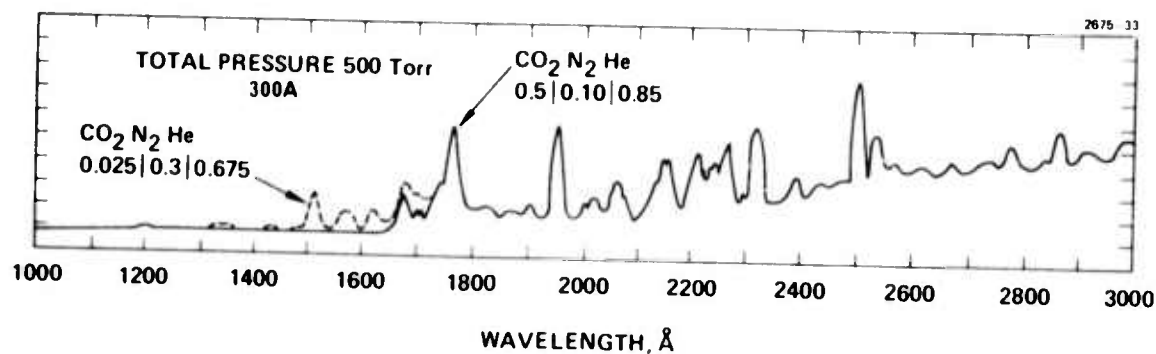


Fig. 32. Relative emission spectra of two CO₂/N₂/He laser mixtures at 300 amps.

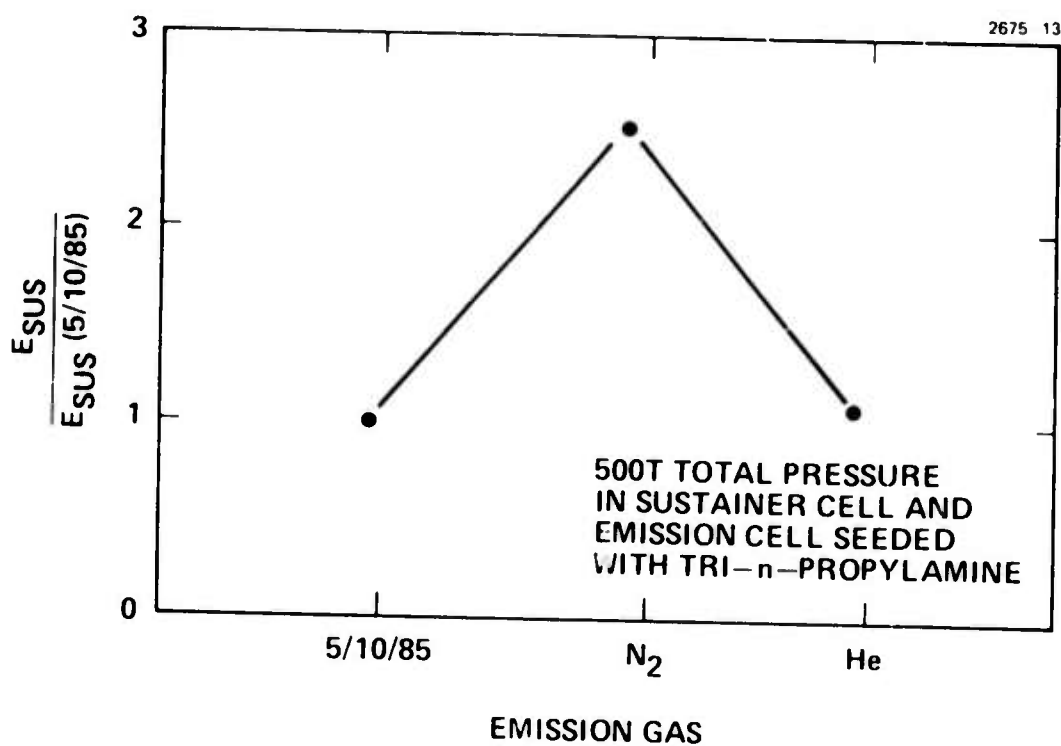


Fig. 33. Sustainer energy measurements obtained using different emission gases.

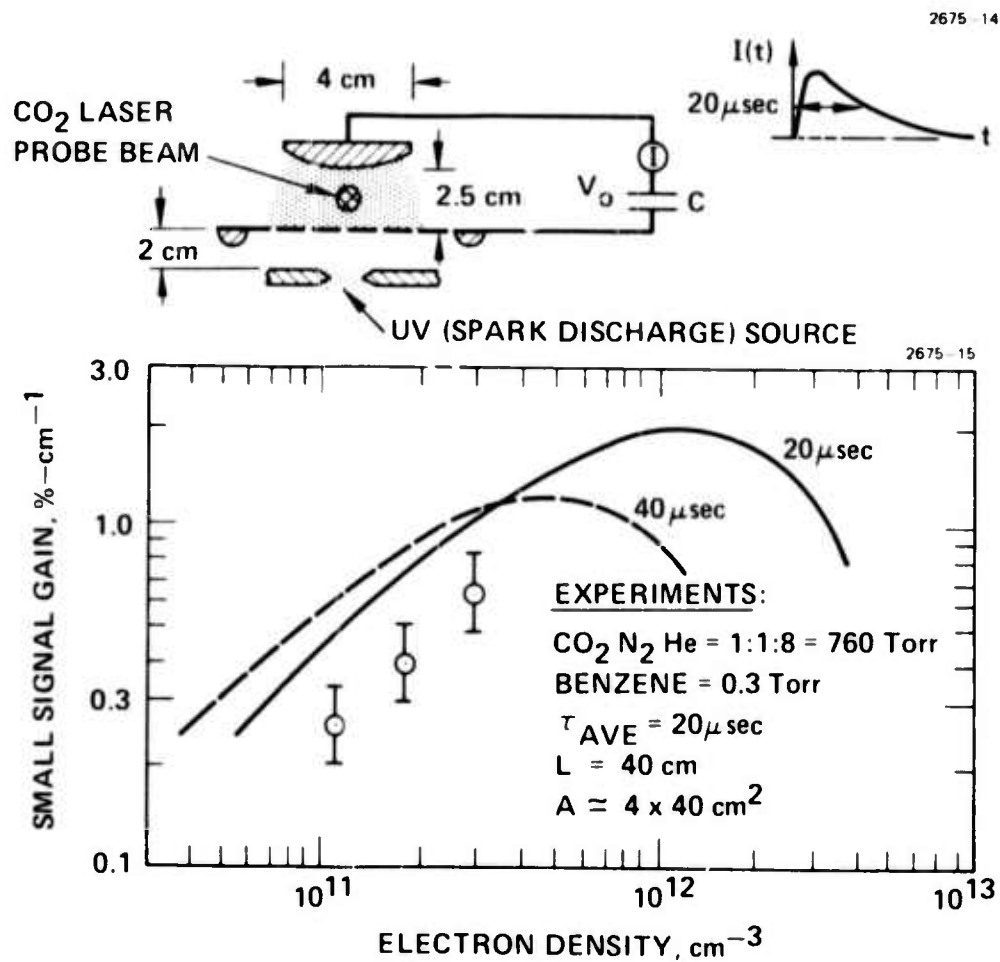


Fig. 34. Gain measurements in UV sustained CO₂ laser.

IV. CONCLUSIONS AND FUTURE PLANS

The results obtained to date are encouraging indicators that UV sustained plasma discharges can indeed be successfully produced and will probably be scalable to large sizes.

The information as to the optimum laser mixture and optimum seed gas concentration presented will be incorporated in an effort to obtain laser output data using a large scale testbed ($2.5 \times 2.5 \times 40 \text{ cm}^3$) during the remaining portion of the contract.

In particular, during the remaining months of the program, work will be undertaken in the following areas:

- Parametric study of laser output data
- Small signal gain measurements for various $\text{CO}_2/\text{N}_2/\text{He}$ laser mixtures
- Current density measurements with a flashlamp source replacing the spark sources
- Tailoring the spectra of the flashlamp source for efficient matching with the absorption spectra of gas additives
- Investigate different seed gases
- Obtain metal vapor spectra.